

Master degree course in Electronic Engineering

Master Degree Thesis

LoRa[®]: applications and validations in complex urban environment



**POLITECNICO
DI TORINO**

Supervisors

Prof. Marco ALLEGRETTI

Prof. Ladislau MATEKOVITS

Candidate

Luca MATTIAUDA

ACADEMIC YEAR 2019-2020

This work is subject to the Creative Commons Licence

Ringraziamenti

Mi è doveroso dedicare questo spazio del mio elaborato alle persone che hanno contribuito, con il loro instancabile supporto, alla realizzazione dello stesso.

In primis, un ringraziamento speciale ai miei relatori, Prof. Matekovits Ladislau e Prof. Allegretti Marco, per i loro indispensabili consigli, per l'attenzione e la disponibilità che mi hanno dedicato durante tutto il percorso di stesura dell'elaborato.

Ringrazio infinitamente i miei genitori che mi hanno sempre sostenuto, appoggiando ogni mia decisione, accompagnandomi in questo percorso.

Un grazie di cuore a tutti coloro che mi sono stati vicini, nei momenti tristi e felici, con il loro affetto e amicizia. E' anche grazie ai loro preziosi consigli che questo lavoro è stato possibile.

Un ringraziamento particolare va ad Anna e Fabio.

Infine, dedico questa tesi a me stesso, ai miei sacrifici e alla mia tenacia che mi hanno permesso di arrivare fin qui.

Contents

Contents	1
List of Figures	3
List of Tables	5
Nomenclature	6
Abstract	8
1 Introduction	1
1.1 Background	1
1.2 Objectives and Contributions of the Thesis	2
2 Spread Spectrum Modulations	4
2.1 Direct Sequence Spread Spectrum	5
2.2 Frequency Hopping Spread Spectrum	7
2.3 Chirp Spread Spectrum	8
3 LoRaWAN Protocol	11
4 Applications	15
4.1 Healthcare	15
4.2 Environmental Monitoring	16
4.3 Disaster Prevention	17
4.4 Farming	18
4.5 E-mobility	18
4.6 Smart City	19
4.7 Satellite Communication	21
5 Characteristics of Devices	22

6	Preliminary Propagation Simulation	24
6.1	Path Loss Models	24
6.1.1	Free Space Path Loss Model	24
6.1.2	Longley-Rice Path Loss Model	25
6.1.3	Okumura-Hata Path Loss Model	32
6.2	Comparison between Path-Loss Models	33
6.3	Simulation	37
6.3.1	Scenarios	37
6.3.2	Results	39
6.3.3	Final Observation	46
7	Measurements	47
7.1	Results for outdoor path loss	48
7.2	Results for indoor path loss	51
7.3	Final Observation	55
	Conclusions	57
	References	59

List of Figures

2.1	Example of DSSS application	6
2.2	Eight cells LFSR	7
3.1	LoRa Packet format	11
3.2	LoRa Uplink Packet Format	13
3.3	LoRaWAN topology	14
6.1	Transmission path	27
6.2	Transmission paths for TX1A	33
6.3	Transmission paths for TX1B	34
6.4	TX1A LOS path	34
6.5	TX1B obstructed path	35
6.6	Comparison between different empirical models for path loss attenuation.	35
6.7	Course of the land along obstructed path.	36
6.8	<i>Scenario 1</i>	38
6.9	<i>Scenario 2</i>	38
6.10	<i>Scenario 1</i> : TX1B, Output Power: 20 dBm, Receivers Height: 1 m	39
6.11	<i>Scenario 1</i> : TX1B, Output Power: 11 dBm, Receivers Height: 1 m	40
6.12	<i>Scenario 1</i> : TX1A, Output Power: 11 dBm, Receivers Height: 1 m, 8m for RX3.	41
6.13	<i>Scenario 1</i> : TX1A & TX1B, Output Power: 11 dBm, Receivers Height: 1 m, 8m for RX3.	41
6.14	<i>Scenario 2</i> : TX2A, Output Power: 11 dBm, Receivers Height: 10 m.	42
6.15	<i>Scenario 2</i> : TX2A, Output Power: 14 dBm, Receivers Height: 4 m.	43
6.16	<i>Scenario 2</i> : TX2B, Output Power: 11 dBm, Receivers Height: 8 m.	43
6.17	<i>Scenario 2</i> : TX2B, Output Power: 14 dBm, Receivers Height: 4 m.	44
6.18	<i>Scenario 2</i> : Coverage of <i>Scenario 2</i>	45
7.1	Coverage accordingly to Longley-Rice model	49
7.2	Receiving points	50

LIST OF FIGURES

7.3	Outdoor Path Loss	50
7.4	CDF of the deviation from predicted attenuation value (in dB)	51
7.5	Coverage of the indoor area	52
7.6	Indoor path loss (LOS)	53
7.7	CDF of the deviation from predicted attenuation value, in dB (LOS). .	53
7.8	Indoor path loss (NLOS).	54
7.9	CDF of the deviation from predicted attenuation value, in dB (NLOS)	54

List of Tables

3.1	ISM frequency band characteristics for Europe and Northern America	11
5.1	Comparison within modules performances in application presented in literature. Results taken from [15].	22
5.2	Semtech modules parameters. Data taken from [99–101]	23
6.1	Typical value of δh	25
6.2	Path Loss Methods comparative table for fixed distances.	36
7.1	LoRa parameters set-up for outdoor communication.	48
7.2	LoRa parameters set-up for indoor communication.	51
7.3	Comparative table for LOS and NLOS models.	55

Nomenclature

R_c	Chip rate
R_s	Symbol rate
LUT	Look Up Table
CSS	Chirp Spread Spectrum
ADR	Adaptive Data Rate
AES	Advanced Encryption Standard
GHG	Greenhouse Gases
LoRa	Long Range
LPWAN	Low Power Wide Area Network
LTE	Wideband Code Division Multiple Access
NB-IoT	Narrowband Internet of Things
TFP	Total Factory Product
WCDMA	Wideband Code Division Multiple Access
CDF	Cumulative Distribution Function
CSS	Chirp Spread Spectrum
DSSS	Direct Sequence Spread Spectrum
EIRP	Equivalent Isotropic Radiated Power
FHSS	Frequency Hopping Spread Spectrum
GDP	Gross Domestic Product

NOMENCLATURE

GPS	Global Positioning System
ICT	Information and Communication Technology
IoT	Internet of Things
ISM	Industrial Scientific Medical
LEO	Low Earth Orbit
LFSR	Linear Feedback Shift Register
M2M	Machine to Machine
PG	Processing Gain
PN	Pseudo Random Noise
RSSI	Received Signal Strength Indicator

Abstract

The large number of technologies that can be used in the Internet of Things (IoT) (LoRa, Sigfox, Nb-IoT, Wi-Fi,...) can lead to undoubted benefits in many areas. For example the use of a Wireless Sensor Network (WSN) can lead to a decrease in polluting emissions or to an improvement in a company's revenues due to a careful and automated management of resources. The presence of different technologies with different protocols that are used within the same field leads to the need of a standardization. The Long Range (LoRa) technology, and its protocol Long Range Wide Area Network (LoRaWAN), is standing out among others due to its low power consumption and long communication range. The presence in the literature of a large number of papers that test the LoRa technology and that study its applications in various fields, attests to how this technology is leading in the IoT field. In this work, firstly, a comprehensive review of scientific articles has been conducted. This study focused on which use-cases were feasible with the LoRa communication technology. The selected papers have been divided into seven macro areas, taking into account the different applications: healthcare, environmental monitoring, disaster prevention, farming, e-mobility, smart city and satellite communication. Particular attention has been given to applications in urban environment for which a higher amount of papers are available in the scientific literature. An investigation on the last trend on devices which make use of the LoRa communication has been also carried out. This survey lead to a publication ¹. In the second part of this thesis numerical simulations have been carried out with the aim to verify the possibility to cover two specific areas of interest, namely a neighbourhood in a city and an inhabited stretch of coast. The characteristics of the TTGO LoRa32 board have been considered as transmitting and receiving nodes. The simulations put on display how the terrain configuration could affect the covering range but models that take into consideration building diffraction predict higher attenuation. In the last part several measurement of RSSI have been taken in a sub-urban area in order to drawn a proper path loss prediction model for the LoRa communication which has been compared with general models for wireless communication both in indoor and in outdoor scenarios.

Luca Mattiauda
November, 2020

¹L. Carosso, L. Mattiauda, M. Allegretti, *A Survey on Devices Exploiting LoRa Communication*, Acta Marisiensis. Seria Technologica, Vol.18 no. 2, p. 31-35, 2020

Chapter 1

Introduction

1.1 Background

Many studies have affirmed that the world is on a new wave of innovation thanks to ICT (Information and Communication Technologies), in particular focusing on its application in M2M (Machine to Machine) communication, that is what is intended by IoT (Internet of Things) [1]. By the year 2024 there are expected to be at least 20 billion devices belonging to the IoT family [2].

The global revenue related to IoT and its applications (just to name few: automated warehouse, health-care, smart cities, environmental monitoring) have an estimated swelling of \$3.900-\$11.100 trillion by 2025 [3]. Although this prevision has been done before the COVID-19 pandemic that has severely affected the world economy [4], it is possible to consider IoT as a way to help the economy for a fast recovery [5]. In fact, in [1], on a sample of 85 countries around the world, a direct link between the number of IoT connections and TFP (Total Factory Product) has been observed, which is contemplated as directly related to GDP growth rate [6].

In everyday consumers life, IoT could drastically change how goods and services have been traditionally used. A very popular example are Smart Homes where users have the opportunity to control many devices (some of which are typically not connected) comfortably via wireless while other aspects are fully automated based on collected data, such as smart energy management [7]. Moreover saving energy and reducing environmental impact have proved to be increasingly popular topics within consumers, as well as being a real threat. A study over 12 000 people around the world showed that 46% of them believe that technological innovation would help them in being more eco-friendly, in particular, 36% see in ICT the best solution [8]. GHG (Greenhouse Gases) emissions have to be reduced by 40%-70% to maintain the global temperature increase under 2°C [9]. IoT technologies could help in reducing GHG both indirectly (optimizing resources management in industries) and directly

(via specific sensors used to monitor pollutants); in best-case scenarios, ICT may lead to a reduction of 12% of GHG emission by 2030 [10]. Industries that have already deeply invested in IoT technologies not only claim a decreasing in emissions level but also a better workplace for employees since many pieces of machinery can be connected with no cables in the way [11].

The flexibility to easily add, move and remove wirelessly connected sensors, low power, low cost, and small size platforms are the strength that will lead to an IoT connection density of 10^6 devices in a km^2 [12].

At the moment there is not an unique standard for IoT communications; a first distinction between major ICT used for IoT could be done based on some characteristics [13]:

- Regular Coverage (WI-FI, Bluetooth, Zigbee);
- Deep Coverage
 - Licensed Band (GSM, WCDMA, LTE, NB-IoT)
 - Unlicensed Band (Sigfox, LoRa)

1.2 Objectives and Contributions of the Thesis

As mentioned in the previous section, IoT technologies will be increasingly present in people's everyday life. This work will focus on the LoRa communication, the physical layer proprietary technology developed by Semtech, and its protocol LoRaWAN. As yet there are over 100 million devices using LoRaWAN protocol on the globe and it is expected that 43% of overall LPWAN to be based on LoRa by 2023 [14], making it one of the leading technologies in the LPWAN sector.

Three are the points on which this work is intended to linger:

- In what areas and in what way the LoRa telecommunications could affect the World around us?
- Which is the current trend regarding devices that support the LoRa communication?
- Would the LoRa telecommunication be suitable to cover an urban area and how the terrain could affect the communication?
- How the measured path loss for the LoRa communication differs from the most used general path loss models, both for indoor and outdoor applications?

In the first part of the thesis, through a systematic review of the scientific literature, it was wanted to define the applications in which this communication has been applied. Moreover, it has been investigated, selecting the latest publications, which were the most used devices and its performances. From this last review, in collaboration with Prof. Allegretti Marco and PhD Carosso Lorenzo, it has been drawn an article published by *Sciendo* in *Acta Marisiensis. Seria Technologica Vol. 18 no. 2, p. 31-35, 2020.*

IEEE and MDPI were the main databases from which the scientific articles have been selected for the surveys.

In the following different Matlab scripts have been developed to implement dissimilar propagation scenarios in two different areas: a neighbourhood and an inhabited stretch of coast. The simulation has been done exploiting the *MATLAB RF Toolbox* which take into account the Longley-Rice Path Loss prediction model that has been deepened and compared with the empirical Okumura-Hata Path Loss model. The first model takes into account attenuation due to terrain, while the second one the attenuation due to buildings. Since one of the main aspect of the IoT is the ease of use and installation, for the simulation have been taken into account off-the-shelf product parameters.

In the last chapter several measurements of received power have been taken in an inhabited area both indoor and outdoor. Empirical prediction models have been drawn and compared with general models and results present in scientific literature.

This work is structured as follows: in Chapter 2 an overview on the spreading spectrum modulations, focusing on the one exploited by the LoRa physical layer, is presented; in Chapter 3 some key points of the LoRaWAN protocol are described; in Chapter 4 has been provided the literature review focusing on LoRa applications; in Chapter 5 the results of [15] regarding the trend on LoRa modules have been presented; in Chapter 6 the simulation results are reported, after having deepened some path loss models for outdoor transmission; in Chapter 7 are presented the measurement and the derived path loss; in the last chapter there are the conclusions.

Chapter 2

Spread Spectrum Modulations

In single carrier modulation, signals are transmitted with a very narrow band. This is due to the fact that band is a limited resource, especially in the unlicensed zone. On the contrary there are modulation techniques that exploit all the available band ensuring that many users can share same channel without interference between them. Recalling the Shannon-Hartley capacity formula [16]:

$$C = B \log_2 \left(1 + \frac{S}{N} \right) \quad (2-1)$$

And considering that for a spread spectrum modulation usually $\frac{S}{N} \ll 1$ the equation above can be rewrite using Maclaurin expansion for logarithm:

$$C = B \frac{\ln \left(1 + \frac{S}{N} \right)}{\ln(2)} = B \frac{\frac{S}{N} - \frac{(\frac{S}{N})^2}{2} + \frac{(\frac{S}{N})^3}{3} - \dots}{\ln(2)} \quad (2-2)$$

$$\frac{C}{B} \approx 1.443 \frac{S}{N} \quad (2-3)$$

where:

- C : bit rate;
- B : bandwidth;
- $\frac{S}{N}$: signal-to-noise ratio.

So, given a fixed signal-to-noise ratio, the bandwidth is the only parameter free to be changed.

Since, as said, $\frac{S}{N}$ is low, in order to have high bit rate B needs to be large.

2.1 Direct Sequence Spread Spectrum

The Direct Sequence Spread Spectrum (DSSS) modulation has been widely used both in military and private applications in last years [17].

Key point is that symbols are modulated by being multiplied by a bipolar signal representing a code uniquely defined for each users. Each pulse of the code is called chip with duration T_c , and given that T_c is lower than symbol time T_s , the resulting bandwidth is much larger. This code is called spreading code and each chip has value 1 or -1.

The spreading code must be known both at transmitter and receiver sides, in this way demodulation is simply done multiplying again the received signal by the same code and initial symbol is recovered.

Spreading code must satisfy some properties [18]:

- Balance: Number of 1s and -1s inside the code must be as much as possible the same;
- Shifting: A delayed version of a code must satisfy the same properties as starting one;
- Correlation: auto-correlation and cross-correlation are used in order to perform some controls, for example synchronization, level of interference, etc;
- Orthogonality: key point, orthogonal codes can be transmitted over the same channel without interfering between them.

The described encoding allows a large number of users to use the same frequency band, passing from a serial communication to a parallel one. Moreover, exploiting DSSS, narrow band interference inside broadband can be easily reject during demodulation [19]. At receiver side the signal is again multiplied by the spreading code, despreading the desired signal on band B , while every other narrowband interference are spread all over the available bandwidth W_{ss} ; then after filtering it, most of the unwanted signal is discharged. The ability to reject narrow band interference is approximately measured by the Processing Gain (PG) defined in [20] as:

$$PG = \frac{W_{ss}}{B} \tag{2-4}$$

The PG can be used as a qualitative indicator of interference rejection.

There are different families of codes that satisfy the the previous requirements [18].

First example are Hadamard codes generated from Walsh matrix where columns, or rows, are orthogonal vectors of ones and minus ones. These vectors are used as spreading codes and each element is a chip. Unfortunately cross-correlation between shifted version of these codes is no more zero [21].

Another example could be Pseudo Random Noise (PN) sequences. These codes are generated by a Linear Feedback Shift Registers (LFSR) with L cells. In this way $2^L - 1$ orthogonal sequences can be obtained. Two PN sequences generated by two different LFSR with the same number of cells and different feedback taps, can be added giving a Golden Sequence. In this way cross-correlation can be lowered [22].

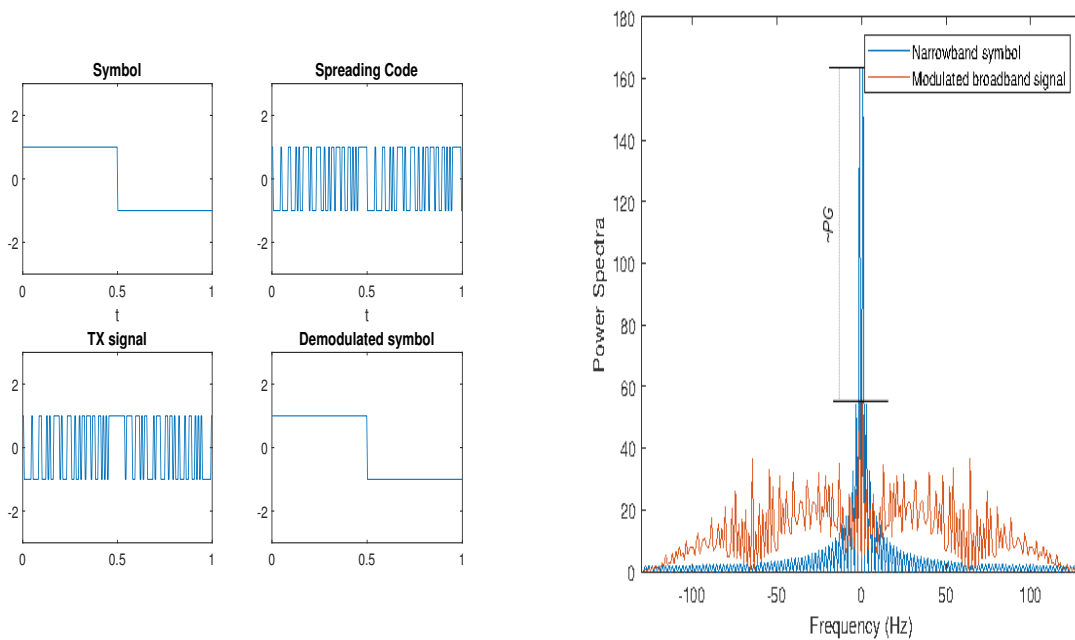


Figure 2.1: Example of DSSS application with PN code

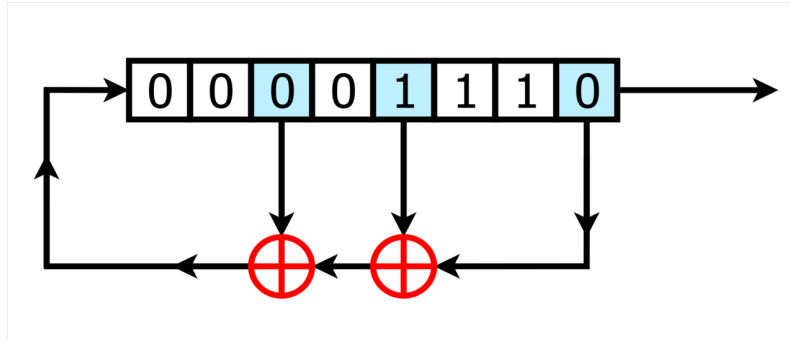


Figure 2.2: Example of LFSR with 8 cells - By Jrme Desroziers - Own work, CC BY-SA 3.0, retrieved from https://commons.wikimedia.org/wiki/File:LFSR_Fibonacci_8_bits.png

2.2 Frequency Hopping Spread Spectrum

The Frequency Hopping Spread Spectrum (FHSS) strategy is mainly used in unlicensed band, especially in Bluetooth application, in order to avoid interference between users in same bandwidth [23].

FHSS makes signal hop between different carrier frequencies (taken from an hopset) chosen in a pseudo-random way. For each carrier a burst of data is sent for a time called hopping period, and each symbol is modulated via traditional narrowband modulation (such as FSK).

If a complete symbol is sent in a channel before the following hop, that's a slow frequency hopping.

The overall order of carrier frequencies sweep must be known at receiver side in order to de-hop the modulated signal. Also in this case it is possible to define the PG as $\frac{W_{ss}}{B}$ [24].

With FHSS modulation the signal is protected against wide band interference while narrowband interference inside a channel during frequency sweeping could be harmful [19].

2.3 Chirp Spread Spectrum

The Chirp Spread Spectrum (CSS) modulation is the one implemented by LoRa. The spread spectrum propriety is assured in CSS modulation by exploiting a sinusoidal signal with linear continuous varying frequency within f_{min} and f_{max} , that is a chirp pulse. The range f_{min} to f_{max} it is what defines modulation bandwidth. If the frequency changes upward, the pulse is an up-chirp, while if it decreases it is a down-chirp.

Widely used in radar application due to good resilience to Doppler effects [16, 25], it has been widely proofed that CSS modulation has good properties also in rejecting narrowband and broadband interferences [16, 26, 27].

The CSS PHY has been described in IEEE 802.15.4, standard for low rate LPWAN networks involving long lasting battery supplied devices. This standard comes after the 802.15.1 inspecting Bluetooth and after 802.15.3 for high rate WPAN. In [28] it is described a transmitter exploiting CSS modulation associated with a differential-QPSK modulation; than each symbol is modulated with both up and down chirp (it is different for the LoRa modulation which only uses up-chirp for payload). A preamble of at least 6 bits is requested for synchronization.

Three parameters are fundamental:

- B : bandwidth $f_{min} - f_{max}$;
- SF : spreading factor (7...12);
- f_c : central frequency.

Focusing on LoRa modulation, which is patented and there is a lack of in depth description of working principle, it is possible to start from the high level description in [16] where it is stated that $R_c = B$ and each symbol of time length T_s is encoded into 2^{SF} chips.

This means that a set of $2^{SF} - 1$ symbols can be represented and therefore SF is the same as the number of bits per symbol.

That means:

$$R_s = \frac{B}{2^{SF}} \tag{2-5}$$

$$T_s = \frac{2^{SF}}{B} \tag{2-6}$$

$$R_b = SF \frac{2^{SF}}{B} \tag{2-7}$$

The Symbol mapping is done by chopping symbols into 2^{SF} equi-lasting chips and re-arranging these samples in a circular shifting way. In such wise each transmitted symbol is modulated into a chirp starting from a $f_i = f_{min} + \delta$ (different for each symbol) and after reaching f_{max} it folds back to f_{min} and rises again to f_i . It's the initial frequency shift that really encode each symbols [29][30][31].

Regarding inter-symbol and inter-channel interference some observation can be dawn looking at orthogonality between symbol belonging to same symbol set and correlation between different channels.

Given the above considerations, the general equation for a CSS symbol can be written as:

$$s_i, k(t) = e^{j2\pi f_i(k,t)t} \quad (2-8)$$

where i indicates the symbol set, k is the symbol index and $f_i(k, t)$ can be defined as :

$$f_i(k, t) = \begin{cases} \frac{B_i}{ts_i} + \frac{B_i}{2^{SF_i}} k & \text{if } t < t_{i,k} \\ \frac{B_i}{ts_i} + \frac{B_i}{2^{SF_i}} k - B_i & \text{if } t \geq t_{i,k} \end{cases} \quad (2-9)$$

and $t_{i,k}$ is the time the chirp need to reach f_{max} , peculiar for each symbol.

In order to verify inter-symbol orthogonality two different symbols are taken from the same set, resulting in having same bandwidth B , same symbol time t_s , same SF , different k . Supposing $t_{k1} < t_{k2}$:

$$\begin{aligned} & \int_0^{t_s} s(k_1, t) s^*(k_2, t) dt = \\ & \int_0^{t_s} e^{j2\pi f(k_1,t)t} e^{-j2\pi f(k_2,t)t} dt = \\ & \int_0^{t_{k1}} e^{j2\pi(\frac{B}{ts} + \frac{B}{2^{SF}} k_1)t} e^{-j2\pi(\frac{B}{ts} + \frac{B}{2^{SF}} k_2)t} dt + \\ & \int_{t_{k1}}^{t_{k2}} e^{j2\pi(\frac{B}{ts} + \frac{B}{2^{SF}} k_1 - B)t} e^{-j2\pi(\frac{B}{ts} + \frac{B}{2^{SF}} k_2)t} dt + \\ & \int_{t_{k2}}^{t_s} e^{j2\pi(\frac{B}{ts} + \frac{B}{2^{SF}} k_1 - B)t} e^{-j2\pi(\frac{B}{ts} + \frac{B}{2^{SF}} k_2 - B)t} dt = \\ & \int_0^{t_{k1}} e^{j2\pi(\frac{B}{2^{SF}}(k_1 - k_2))t} dt + \int_{t_{k1}}^{t_{k2}} e^{j2\pi(\frac{B}{2^{SF}}(k_1 - k_2) - B)t} dt + \int_{t_{k2}}^{t_s} e^{j2\pi(\frac{B}{2^{SF}}(k_1 - k_2))t} dt \end{aligned}$$

The equation above is equal to zero only when $k_1 - k_2$ is equal to the square root of an integer multiple of SF [31].

Nevertheless, in [32] it is reported that Semtech declared that in its modules the orthogonality within chirps is assured by means of Look Up Table (LUT) which are closed-sources.

On the other hand it is not so trivial to demonstrate orthogonality between symbols in different channels. In [33] it is demonstrated that chirps which have different slopes in the frequency characteristic (different bandwidth and different symbol time) are orthogonal.

A description for CSS demodulation can be found in patent [34] and it is quite straightforward: after sampling the received chirp signal a conjugate chirp is generated and multiplied by receiving signal. Doing that, constant frequencies sequences are obtained and computing the *argmax* of the FFT it is possible to recover original symbols values.

In terms of error performances it has been studied in [29] that in a pure AWGN channel the LoRa modulation has same behaviour as FSK, whilst in a fading channel the FSK performances are much worst compared with LoRa ones. Moreover the broadband characteristic makes it resistant to multipath.

Chapter 3

LoRaWAN Protocol

LoRa communication exploit the Industrial Scientific Medical (ISM) frequency band, which follows regional regulations:

Table 3.1: ISM frequency band characteristics for Europe and Northern America

	Europe	North America
Frequency Bands	867-869 MHz	902-928MHz
Channels	10	90
Channel BW Up	125/250kHz	125/250kHz
Channel BW Dn	125kHz	500kHz
TX Power Up	+14dBm	+30dBm
TX Power DN	+14dBm	+27dBm
SF Up	7 to 12	7 to 10
Data Rate	250bps to 50kbps	980bps-21.9kbps
Link Budget Up	155dB	154dB
Link Budget Dn	155dB	157dB

Under these regulations, also normative on packets air-time are depicted. Each packet has the following general format [35]:

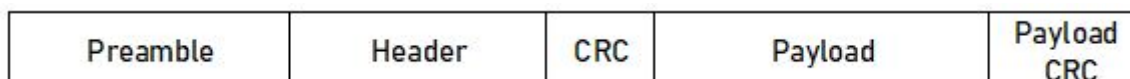


Figure 3.1: LoRa Packet format

The time on air is computed as [35]:

$$T_{packet} = T_{preamble} + T_{payload} \quad (3-1)$$

$$T_{preamble} = (n_{preamble} + 4.25)T_{sym} \quad (3-2)$$

$$T_{payload} = payloadSymbNb \cdot T_{sym} \quad (3-3)$$

$$payloadSymbNb = 8 + \max(\text{ceil}(\frac{8PL - 4SF + 28 + 16 - 20H}{4(SF - 2DE)}(CR + 4)), 0) \quad (3-4)$$

where:

- PL is the payload bytes;
- SF is the spreading factor;
- $H = 0$ or 1 if header is present or not;
- $DE = 0$ or 1 if low data rate is enabled or not;
- CR is the coding rate.

In [36] it is specified how LoRa networks can be distinguished into three classes based on how uplink and downlink are managed in time (all classes admit bidirectional communication between transceivers).

- **Class A:** it is the best choice in terms of power consumption. Downlink is only possible in two short time windows after an uplink is detected. If the packet is completely received along the first receiving window, the second one will not be open. Class A is the most suitable choice for application where uplink communication is preferred.
- **Class B:** Devices of Class B open more windows for downlink with respect to Class A devices.
- **Class C:** Class C devices continuously open receiving windows that are closed during transmission only.

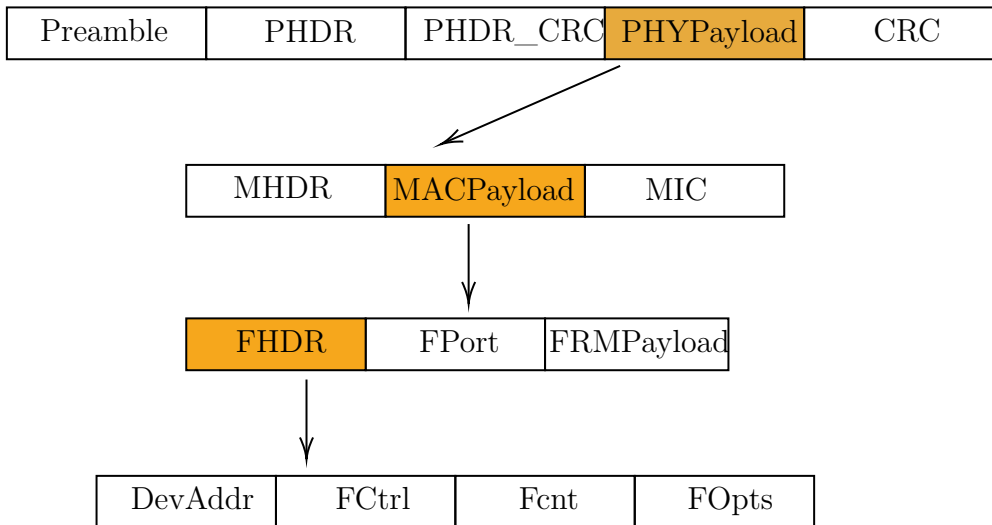


Figure 3.2: LoRa Uplink Packet Format

In the following part of this chapter briefly description of the LoRaWAN protocol is presented, with greater consideration for Class A devices. All the following information is taken from [36], unless otherwise specified.

The LoRa uplink packet is formed by a preamble, an header (PHDR), an header CRC (PHDR_CRC), the payload, and a CRC payload.

In turn, the payload contains a one byte MAC header (MHDR), a MAC payload (MACPayload), and a four byte message integrity code (MIC). The MAC payload size range from 7 bytes to M bytes, where M is region specific.

Since LoRaWAN uses eight different type, of message, the MAC header indicates which type is used.

The MAC payload is composed by a frame header (FHDR) and two optional fields. Inside FHDR there is the end-device address (DevAddr), a one byte control field (FCtrl), a two byte frame counter (FCnt), and a fifteen byte field for frame options (FOpts). Within the FCtrl it is possible to set the bit that activate the adaptive data rate (ADR). Exploiting ADR, the network will self regulate in terms of data rate and power. When the gateway pass the received packet to the network server via IP standard, it is added information about received power and time-on-air. Based on that information, the server will change end device SF in order to optimize the performance. End devices that are near gateway do not need high air-time, so a lower SF and an higher data rate can be used; on contrary, far end-devices will require higher SF and more power.

When ADR is active, each uplink increments ADR_ACK_CNT counter up to a fixed limit, instead, each downlink resets this counter. When the ADR_ACK_CNT reach its limit, the end-devices asks for acknowledgement in FCtrl. If no downlink

is received after a certain amount of time, the end-device return to default data rate value in order to re-gain connectivity.

The network server can control end-devices via MAC commands. MAC commands can be content of FRMPayload field or FOpts, but in the same packet only one of the two choice is possible. When the MAC command is in FRMPayload, FPort is set to 0.

Some of MAC command could be: set end-devices to default parameters, validate connectivity, change of frequency and data rate, request status information of end-devices, configuring delay between uplink and downlink windows, etc..

To assure security, the payload is encrypted using AES encryption with a 128 bits key described in [37]. The key used is different for each end-device.

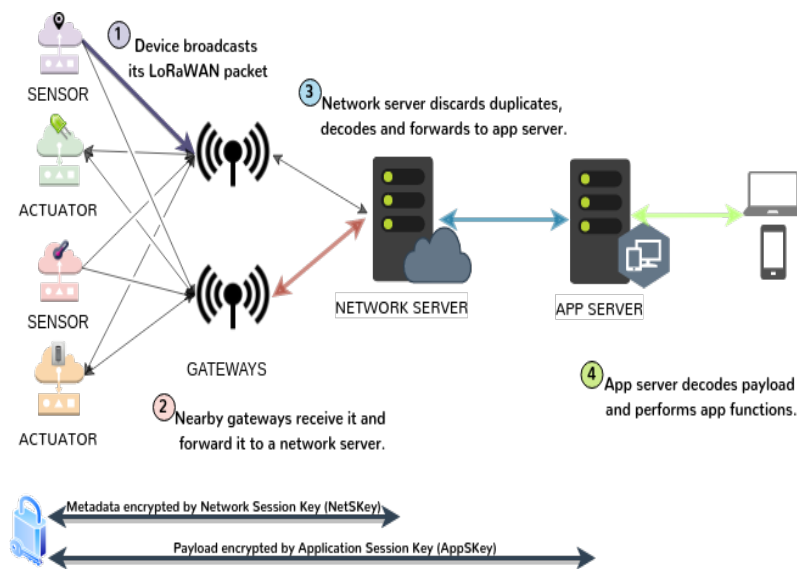


Figure 3.3: LoRaWAN topology - By Brivadeneira Own work, CC BY-SA 4.0, retrieved from [38]

Chapter 4

Applications

4.1 Healthcare

Clinical monitoring is moving from hospital to people houses not only to tracking disease, but also to monitoring various biological parameters for an healthier life.

Just thinking of how common smart watches are becoming it is easy to understand how IoT can improve the health care system sending data from home sensors to experts that can make diagnosis and therapeutic plans.

Tele-medicine can be particularly helpful in situation where patients have some impairment in moving frequently in hospitals, for instance elderly people, disables or in presence of chronic severe ill.

LoRa technology is one of the best choice since most sensors are battery supplied and fast data rate is of no great importance since feedback must be sent only when monitored parameters deviate from normal values [39].

Accordingly to United Nations 16% of world population will be older than 65 years old [40] by 2050, while in Italy, by same year, it is expected to have 36% of people 65 years old or older [41]. Within this age group 10% is affected by Alzheimer's dementia [42]. People with Alzheimer have been observed to have wandering behaviour and tend to get lost (about 40% of patients with such disease) [43]. Tracking IoT devices can be used to track them and detect fall so to inform caregivers and achieve faster actions.

In [39] a cane for elderly people has been developed and tested , equipped with an accelerometer, a GPS and a LoRa transceiver, which main objective was to communicate to a base station the need of help in case of fall. It has been demonstrated that using $B = 500\text{kHz}$, $CR = 4/5$, $SF=7$ a robust communication has been obtained in a city environment (reaching a distance of 1 km with a packet loss less than 20%). A similar board integrated in a small box has been developed in [44]. In this study range has been preferred over data rate (maximum SF has been used)

getting about 12 km communication between nodes.

60% of death worldwide are due to chronic diseases, which requires to be monitored over time. Moreover these diseases can make prohibitive to patients moving to hospitals for analysis. End devices supported with sensors for glucose level, oxygen density, heartbeat rate, etc. can be used to monitor patients from home and communicate data to a central server making it possible to experts to access them and taking actions. In [45] the LoRaWAN protocol has been tested for such scope (LoRa has been chosen for power consumption ten times less than GPRS and for the cost ten times lower than GSM networks), positioning a gateway at 12 meters of height in an urban environment. Authors have reached 33 km² of signal coverage in outdoor environment with SF=7, $B=125\text{kHz}$.

It has been observed in [46] that 96,7% of packets have been received in a campus site sent by an end device (supporting pressure and temperature sensors) wore by a person moving both outdoor and indoor; the base station was an antenna placed 24 m high, with SF=12 and BW=125kHz.

In many countries maternal death rate is still a big problem, caused by lack of doctors and difficulty from women in rural area to reach hospitals in time. LoRa platforms can be used to monitor mothers' parameters from home and sending data to hospitals server where the need to send an ambulance will be verified [47].

LoRa temperature sensors have been thought to help in fighting COVID outbreak in a fast temperature screening of people in private and public buildings [48][49]. Moreover LoRa module can be used for monitoring contact between infected and healthy people [50].

4.2 Environmental Monitoring

As said in chapter 1 environmental pollution is a big threat and it is becoming a very popular topic. According to WHO 4.2 million deaths per year are caused by air pollutions, and 90% of people breathe air with pollutants levels higher than guideline limits [51]. Air pollutants can cause cardiovascular and respiratory diseases, and cancers [52]. This is why air quality must be monitored.

Concerning that, many studies employing LoRaWAN networks have been carried out. In [53] a drone has been used carrying sensors for detecting major air pollutant such as PM , CO , NH_3 , NO_2 , VOC , CO_2 . Drones are useful for monitoring air in areas difficult to reach, communication with a central server storing data is done via LoRaWAN transmission. Also in [54] an end node has been mounted on a drone, to track CH_4 emissions over oil fields. Using SF=9, $B=62.5\text{kHz}$ and CR= 4/6, a distance of about 1 km has been reached. In this case, Class C operating mode has been chosen.

In [55] a three-month air monitoring is presented with data coming from eight different static end nodes with 600m of distance between receiver and transceiver.

Authors of [56] reached a maximum message received distance of 12 km in an urban area using SF10. Their work focused on end devices supporting PM sensors placed 3m high on walls of two different schools. Other works also have demonstrated the good reliability in LoRaWAN sensors node for monitoring air pollution in urban areas [57–60].

Furthermore, contamination in water is determinant in affecting people health, also in this case there is the need to monitor pollutants.

In [61] a system of floating nodes is presented. A 100% correct reception has been obtained under 500m of distance between nodes and gateways using SF7, $B=125\text{kHz}$, $CR=4/5$. In [62] a system for nitrate concentration in water monitoring is presented. The LoRaWAN end-nodes are distant 340m from gateways. 98% of packets have been received correctly (No information about LoRaWAN parameters). Further a comparison between power consumption in LoRa-based controller versus WiFi-based ones is presented with a significant reduction of 2.22 times in LoRa case, making LoRa nodes more suitable for being supplied by solar panels (plus batteries, making the service more reliable).

4.3 Disaster Prevention

Earthquakes, floods, volcano eruptions, massive fires, floods, and landslides are disasters that are not predictable in their entirety or in their effective entity. The only way to limit damages is to take action as soon as the signs of a potentially dangerous event arise. Placing sensors in areas at risk and collecting data from them can be a way to be aware of an imminent threat.

In [63] a flood monitoring system using an ultrasonic sensor it has been developed. The sensor node measure the height of a river level. Data is sent to a receiving node 500 meters away and in case of danger an alert message is published on the social network Twitter, using a Raspberry Pi. They experienced no packet loss, with an assigned frequency of 915 MHz which is the one allowed in Mexico where the test has been conducted.

In [64–66] sensor networks able to detect a fire within a forest have been developed. In [64] end-nodes have been equipped with a GPS, fire sensor, LoRa transmitter, and a Raspberry PI, reaching a maximum communication distance of 1.3 km. Unlike all previous works, in [65], authors implemented a LoRaWAN mesh network topology. They equipped four end-nodes with smoke sensors reaching 500 m transmission with settings: B 250, CR 4/5, SF 10. In [66] fifteen transmitting boards have been equipped with temperature, humidity, wind speed, and CO_2 sensors to detect the most favourable conditions for the outbreak of a fire. They covered an area with 1

km radius using SF=7.

A landslide detection system has been studied in [67] using a set of gateways in known locations monitoring some sensors, such as accelerometer and pressure sensor, and tracking their position via trilateration based on Received Signal Strength Indicator .

Moreover, in [68] a system which aim is the surveillance of soil heat around a volcano has been tested. End nodes consist of buried thermometers sending data to a repeater in order to extend the range. It has been used SF = 7 so that air time is reduced, and consequently also power consumption. Authors say that LoRa performances were good with packet loss less than 2% over an all-day monitoring.

4.4 Farming

The capability of the LoRa network to cover a large area with low cost and low power end devices, make LoRa technology very suitable to monitor parameters of a vast cultivated field. Moreover, in these situations, a low data rate is sufficient since no sudden variations are not expected.

In [69] the LoRaWAN has been used to monitor a tree farm. CR, SF, and B have been varied in order to find the best PHY parameters. Every end device has been tested at 100m, 150m, and 200m at a height of 2,5m. It has been observed that in a place where there are many obstacles on the field, such as trees, the best performances have been obtained with higher CR, SF, and transceivers positioned at high height.

Authors of paper [70] designed a communication system for underground-underground communications and underground-aboveground communications in order to keep track of soil specifications. It has been noticed that the quality of transmission deeply depends on soil characteristics, in particular on the permittivity which greatly changes with soil moisture. Wetter soil leads to great degradation. Regarding distance, it has been seen that in under-under case 20m have been reached while 200m in the under-above case.

In [71] a network to control an irrigation system has been developed using SF=10 and CR=4/8 for a 2km range.

Also [72] claims that between all IoT LoRa network in agriculture applications can give good results.

4.5 E-mobility

IoT applied to vehicles can lead to a reduction of traffic jams, high accident rates, pollutant emission, and incorrect behaviours. According to the paper [73], LoRa

transmission can follow objects that move until a velocity of 40km/h; this means that LoRa technology is best suitable for tracking vehicles in crowded ambient where velocity is limited.

While the Global Positioning System (GPS) is a widely used technology for localization it requires a large amount of power, that means large batteries are required and this implies that it is not the best choice for human-powered vehicles which are required to be as light as possible. In [74] and [75] tracking systems involving bikes have been developed using LoRa both as a way of tracking and long-range communication between bikes and stations, the power required by the LoRa shield could be satisfied by a simple dynamo motor [74]. Authors of [75] claimed 100% of packet delivery for different baud rates.

In [76] a packet delivery ratio of 95% has been obtained during tracking of a vehicle moving at a speed of 20km/h in a campus ($SF=12$, $CR=4/5$, $B=125$ kHz); authors faced transmission problems due to the presence of buildings, reaching 1,4km tracking distance.

Some researches over systems designed to minimize car accidents have been carried out employing LoRa plus GPS boards. The data obtained with GPS are then sent via LoRa. Authors of [77] designed a system to avoid car accidents due to damaged roads, involving a speed of 60 - 90 km/h. In [78] a way to avoid crashes during overtaking has been studied, the scenario was a straight road. The studied system alerts the driver when a proximity danger is detected. Communication between vehicles is done via LoRa and it has been got 95% of successful results for a distance less than 200m while 90% of correctness on a distances greater or equal than 800m.

On the way of unmanned electric vehicles, in [79] a way to correctly guide an autonomous vehicle has been studied, providing communication between vehicle and stations along the road reaching a range of 2,5 - 4 km.

4.6 Smart City

Urban environments, due to a large number of people and buildings consist of a very complex set up in IoTs application for the plethora of implementation that such kinds of technologies could appeal. In particular, the feasibility of the LoRa long-range communication in an open space where many buildings are present has been studied in different articles. Prajanti et al. conducted a simulation over a big metropolitan area in order to find the optimum network configuration, finding a range where the packet loss was equal or higher than 90%. They have found that a single gateway could cover a 3 km - 3.5 km radius area and the optimum number of devices should be around 3000 [80]. A more realistic study has been conducted in [81], authors tested a LoRa network in a city, and although the transceiver were placed at 71m height they only reached coverage of 1km - 2km probably due to

the shadowing effect of nearby buildings. Considering a smaller area both [82] and [83] showed how a mesh topology would be better than a star network, the mesh topology can extend the range using a lower SF, that means lowering the air time and so the risk of packet collision resulting in a lower packet loss percentage. In paper [84], authors have experienced a 14 km communication with a packet loss of 75% but must be highlighted that the study case is a port, so a flat plain area with no obstacles over the sea.

Deeping on particular applications in open space over the urban area many articles are present in literature that discusses the IoT network which exploits LoRa communication. In [85] a smart public light system that transmits data to a server via LoRa has been presented. Authors of [86] developed a smart trash bin equipped with an end node which consists of a micro-controller, an ultrasound sensor and a LoRa TX module that communicates when the bin is almost full, in this way the city trash management could be improved in terms of time and cost. The test has been done inside city walls where the maximum reached distance has been 1.1 km with no packet losses. Authors exploited event-driven communication since their main target was low power consumption and estimated a lifetime of 502 days using a 3500 mAh battery.

Another relevant issue in cities is people or vehicle traffic. In [87] a 74 low-cost sensors node network has been installed, aim of the network was monitoring the movement of people; while authors of [88] developed a smart parking system which consists in positioning TX at the center of all parking slots: when a car is parked above a sensor, the RX will sense a significant signal strength drop. Informing car drivers of available parking slots can help lower traffic jam by 30% [89].

Furthermore, cities also have important underground structures, whether they are historic structures or tunnels for pipelines or power supply, which can be monitored using IoTs. In [90] it is presented a linear multi hop LoRa network for monitoring an ancient underground aqueduct, the maximum reached distance between nodes is 200 m. Authors of [91] exploited LoRa transceiver for monitoring heat of a power grid: the gateway was 1.5 m above the ground which communicates with a repeater placed 2 m underground; between them, there was a metallic lid. The authors moved the gateway up to 20 m of horizontal distance and they recorded no packet loss for both SF 7 and 12.

Talking about IoT application in a smart city it is dispensable to consider also indoor communication. Authors of [92] and [93] have conducted a deep analysis of the performance of a LoRa network in different types of buildings, with an eye on fading and coverage. Both studies have been conducted in three scenarios: in a room with TX and RX in line of sight, TX and RX on the same floor but with obstacles between them, TX and RX on different floors. The mentioned studies underline

the fact that increasing the bit rate the coverage is lowered, but decreasing the bit rate increases the time on-air which means higher power is needed. In particular, in [93], authors considered as good LoRa coverage an area where the packet loss was no more than 10%. Authors confirmed that they reached good coverage in an eight floor building, whilst authors of [94] have experienced a packet loss of 78% when fourteen floors were between TX and RX.

4.7 Satellite Communication

In all previous cases, the LoRa networks never exceeded the extension of an urban area. There could be some context where sensors are applied to monitor an area that is much far from a place where a server can be installed. In this optic, a solution is presented in the literature. The main idea is to rely on the LEO satellite. The LEO orbit is between 500 km and 2000 km from the surface and orbit of the satellites are easily predictable with good coverage over the earth and low latency. LEO satellites are designed to be low cost and some studies propose to use these satellites to collect data from ground sensors using LoRa communication. In [95] a study over the adaptability of LoRa protocol in ground-LEO satellite communication has been carried on. Since the communication almost happens in free space the distance is satisfied but the Equivalent Isotropic Radiated Power (EIRP) needed is quite high, so a power higher than the one permitted in ISM frequency should be used. To overcome this problem authors suggest using antenna with high gain. Moreover, the time on-air could reach 7 ms which is no more negligible. Authors of [96] simulated employing a software-defined radio a signal affected by a Doppler effect equal to as a signal received by a satellite orbiting at an altitude of about 200 km which is lower than LEO orbit, that means that also the frequency shift is worst than the one that would be experienced by an LEO satellite. Simulation pointed out the resistance of LoRa communication over the Doppler effect for all SF, in particular with lower SF a more stable communication has been achieved. Although in section 4.7 it has been said that the maximum relative speed between TX and RX is 40 km/h before experiencing heavy degradation in communication, authors of [96] proved that in line of sight condition, and so in absence of multipath fading (which is present in an urban environment,) the speed limit declared in other studies does not apply in satellite communication conditions. In [97] a receiver that would be capable to work on LEO satellite and detect LoRa signals has been designed and simulated. Furthermore, in [98] it is presented how a swarm of satellites can exploit the LoRa communication to exchange information and commands among them.

Chapter 5

Characteristics of Devices

From the survey that has been carried out in [15], it has been seen, from the papers that have been selected, that two are the manufacturers of modules that support the LoRa communication: Semtech (which patented the LoRa physical layer) and Microchip. SX1272, SX1276/8 and SX1261/2 are the ones belonging to Semtech while RN2903 and RN2483 are the modules developed by Microchip.

The survey results are summarized in Tab 5.1 which is derived from the Table 2 in [15] where it is possible to distinguish use-cases and performances for each device.

Table 5.1: Comparison within modules performances in application presented in literature. Results taken from [15].

use-case	Band (kHz)	SF	Central Frequency (MHz)	TX power (dBm)	Range	Module
multifloor communication	500	7	915	10	7 floors (17,5 m)	SX1272
urban static WSN	-	-	868	-	1,1 km	SX1272
urban static WSN	-	-	868	-	350 m ²	SX1276
urban static WSN	-	10	868	-	1 km ²	SX1276
urban static WSN	125	7÷12	923,2-924,6	12	40 m	SX1276
Earth-space communication (monopole antenna)	125	12	915	22	-	SX1262
Earth-space communication (directive antenna)	125	7÷12	915	22	-	SX1262
urban WSN	250	7	868	-	-	SX1261
embedded node	250	7	868	14	-	SX1261
smart house	-	-	915	18.5	-	RN2903
urban WSN	-	7	915	12	1,5 km	RN2903
wearable sensor node	125	7	868	10	1,5 km	RN2483

It is possible to notice that the SX127X series modules are suitable for urban WSN installation, also in indoor use-case, but, when the center frequency is higher, communication suffers from higher attenuation. For this reason the transmitting output power should be increased to reach satisfactory results. The SX126X series modules have been used for LEO communication with a lifetime of more than 4 years. This is justified for their better performance with respect to the SX127X series (Tab. 5.2).

It has been observed that there are not published results on use-cases involving the latest module released by Semtech, the LR1110.

Table 5.2: Semtech modules parameters. Data taken from [99–101]

	SX1272	SX1276	SX1261
Link Budget	157 dB	168 dB	170 dB
RX current	10 mA	9.9 mA	4.6 mA
Sensitivity	-137 dBm	-148 dBm	-148 dBm

Although the majority of applications involve the Semtech products, within the last year researches some studies have been carried out on Microchip modules. It has been seen that they could have good performances in urban environment, also with a slow-moving receiver, whilst there is a reported application in smart house system of the RN2903, performance in correct received packet was low [15].

Chapter 6

Preliminary Propagation Simulation

Aim of this chapter is to verify if the coverage of two real zones, where a WSN has to be installed, is possible with transmission parameters of an off-the-shelves device that exploit the LoRa communication according to the most common path loss models used for outdoor communication. There are different mathematical models that can be used for computing the attenuation that electromagnetic signals may undergo. The models considered are empirical, that means that have been drawn from measured data. The simulation will be carried out exploiting the *Matlab RF Toolbox* which make use of the Longley-Rice Path Loss Model. Since this model only takes into account the diffraction due to the environment (it will be explained in Section 6.1.2) it will be compared with the Okumura-Hata Path Loss Model (Section 6.1.3). Given the significant difference between the two models, when the Longley-Rice is compared with the attenuation obtained from the Okumura-Hata models for the city environment, some precautions will be taken during the setting parameters of the simulation, as it will be explained in Section 6.3.2.

6.1 Path Loss Models

6.1.1 Free Space Path Loss Model

The free space path loss model is valid only in situation for which no obstacles or reflection are considered.

Starting from the Friis equation, a signal of frequency f at distance d in the free

space has an attenuation in dB equal to:

$$\begin{aligned}
 L_{bf}(d) &= 20 \log \left(\frac{4\pi f d}{c} \right) = & (6-1) \\
 &= 20 \log \left(\frac{4\pi}{c} \right) + 20 \log f + 20 \log d = \\
 &= -147.55 + 20 \log f + 20 \log d
 \end{aligned}$$

If the frequency is indicated in MHz and the distance in km, the previous equation can be rewritten as:

$$L_{bf}(d) = 32.45 + 20 \log f + 20 \log d \quad (6-2)$$

6.1.2 Longley-Rice Path Loss Model

The Longley-Rice Path Loss prediction model has been described for the first time in 1968 in [102]. This model has been obtained after thousands of measurements in different environments for a frequency range from 40 MHz to 10 GHz. As explained in annex 3 of [102] the necessary parameters to be known are the carrier frequency (f) in MHz, the path distance (d) in km and the antenna heights from ground (h_{g1}, h_{g2}) in meters. Moreover, authors carried a probabilistic study over earth refractivity index and morphology. Thanks to these studies they have been able also to provide a model to calculate the effective radius of the earth and a factor δh . The effective radius of the earth is a function of the refractivity index for which a local mean annual value has to be considered since it changes with temperature, pressure, humidity, etc. In this way also weather effects are taken into account. Common value is 8493 km which is 4/3 of the actual radius. Instead, the factor δh is related to how the terrain change with respect to the sea level, it depends on the distance but as it increases it converge asymptotically to a constant value. Typical values could be taken from table 1 of [102]:

Table 6.1: Typical value of δh .

	δh (m)
Water	0-5
Smooth plains	5-20
Slitgthly rolling plains	20-40
Rolling plains	40-80
Hills	80-150
Mountains	150-300
Rugged Mountains	300-700

In addition to the four essential inputs: f_c, d, h_{g_1} and h_{g_2} , in order to compute the attenuation, other parameters are needed:

- $h_{e_{1,2}}$ which are the effective antenna heights;
- $\theta_{e_{1,2}}$ which are the elevation angle with respect to the line of sight plane;
- $d_{L_{1,2}}$ which are the distances from the antenna and the horizon obstruction;
- d_L that is the distance between the antennas.

The distances are calculated over an arc with radius equal to the effective earth radius.

When detailed information about the terrain morphology are not given, $h_{e_{1,2}}$, $d_{L_{1,2}}$ and $\theta_{e_{1,2}}$ can be approximated as:

$$h_{e_{1,2}} = \begin{cases} h_{g_{1,2}} & \text{for net-type communication} \\ h_{g_{1,2}} + ke^{-2\frac{h_{g_{1,2}}}{\delta h}} & \text{for antennas on hills.} \end{cases} \quad (6-3)$$

with k equal to:

$$k = \begin{cases} 1 + 4 \sin(\pi \frac{h_{g_{1,2}}}{10}) & \text{if } 0 \leq h_{g_{1,2}} \leq 5, \\ 5 & \text{otherwise.} \end{cases} \quad (6-4)$$

The distance between antennas and line-of-sight obstruction can be computed on a smooth terrain as:

$$d_{L_{s_{1,2}}} = \sqrt{0.002ah_{e_{1,2}}} \quad (6-5)$$

where a is the earth effective radius.

Then, same distance over a non-uniform terrain can be approximated with:

$$d_{L_{1,2}} = d_{L_{s_{1,2}}} e^{-0.07\sqrt{\frac{\delta h}{h_e}}} \quad (6-6)$$

where h_e is equal to:

$$h_e = \begin{cases} h_{e_{1,2}} & \text{if } h_{e_{1,2}} \geq 5, \\ 5 & \text{otherwise..} \end{cases} \quad (6-7)$$

Values of $\theta_{e_{1,2}}$ can be approximated with:

$$\theta_{e_{1,2}} = \frac{5e - 4}{d_{L_{s_{1,2}}}} \left[1.3 \frac{d_{L_{s_{1,2}}}}{d_{L_{1,2}}} \delta h - 4h_{e_{1,2}} \right] \quad (6-8)$$

When the morphology of the terrain is known, the horizon distances are considered as the values that maximize:

$$\theta_{e_{1,2}} = \frac{1e - 3(h_{L_{1,2}} - h_{s_{1,2}})}{h_{L_{1,2}}} - \frac{d_{L_{1,2}}}{2a} \quad (6-9)$$

where $h_{s_{1,2}}$ are the heights of the ground in the antennas locations from the reference level and $h_{L_{1,2}}$ is the height of the line-of-sight obstruction from the reference level. Regarding the reference level, the 4/3 of actual earth radius approximation is still acceptable if $\theta_{e_{1,2}} \leq 0.2$ radians; if not, a reference level equal to a fitting line of the course of the land between the two antennas has to be taken.

Regarding the antennas effective heights, also in this case the approximation are still valid, especially for very uneven terrains. All the previous equations have been taken from the body and annex 3 of [102].

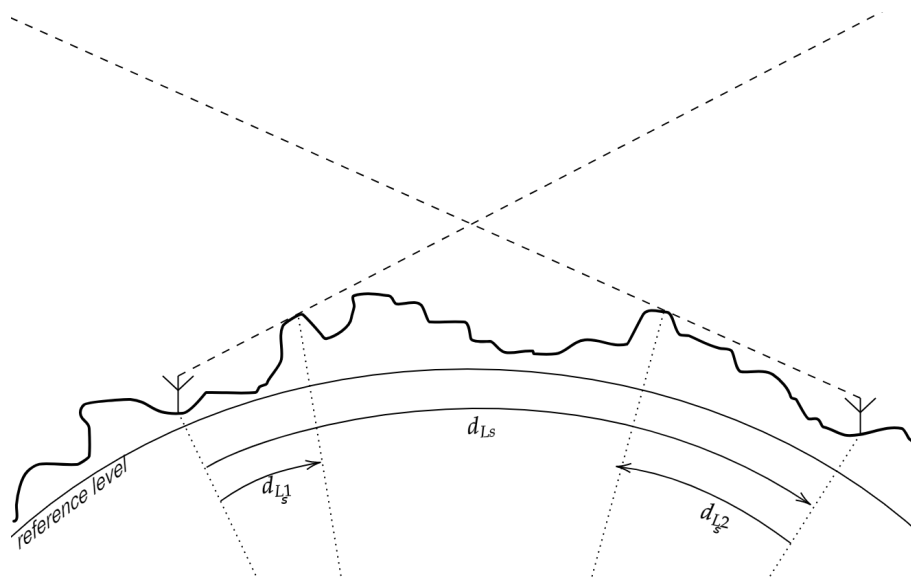


Figure 6.1: Line Of Sight path

The Longley-Rice model takes into account free space losses, diffraction and scattering effects due to terrain without considering buildings or vegetation. Then the model distinguish three zones based on which attenuation effect is predominant. Defining a distance d_x for which diffraction losses are equal to scattering losses, the three regions are:

- region 1 : $d_L < d_{L_1} + d_{L_2}$ antennas are in line-of-sight, two rays scenario is considered;
- region 2 : $d_{L_1} + d_{L_2} < d_L < d_x$ for which diffraction phenomena are predominant;
- region 3 : $d_x < d_L$ for which scattering phenomena are predominant.

The total attenuation, in dB, therefore is:

$$L_{cr} = L_{bf} + A_{cr} \quad (6-10)$$

Assuming matched antennas and omnidirectional radiation, the two rays attenuation can be written as [102]:

$$A_{cr} = -10 \log[1 + R_e^2 - 2R_e \cos(\frac{4.1917e - 5fh_{e_1}h_{e_2}}{d} - c)] \quad (6-11)$$

where c is the phase shift between the two paths and R_e is the effective reflection coefficient.

In the body of [102] it is said that under conditions of: uneven terrain and f higher than 100 MHz, $R_e \cong 0.9$ and $c = 0$. This application is only valid on ground, for transmission over the sea the equations in annex 3 of [102] must be followed. Considering the maximum range of 2 km, the following distances are considered:

- $d_0 = 0.5d_L$
- $d_1 = d_0 + 0.25(d_L - d_0)$

Those distances are used in 6–11 to compute A_{0t} and A_{1t} that are the attenuations due to the two rays scenario. Then, in annex 3 of [102], the term A_e and m_d are also computed. These terms are the intercept and the slope related to the diffraction attenuation curve and takes into account diffraction and clutter effects. In fact, although diffraction is not the predominant cause of losses in region 1, this effects has to be taken into account, especially if terrain is irregular. The diffraction attenuation terms in d_0, d_1 and d_L are:

$$\begin{aligned} A_{od} &= A_{ed} + m_d d_0; \\ A_{1d} &= A_{ed} + m_d d_1; \\ A_{Ls} &= A_{ed} + m_d d_{Ls}. \end{aligned} \quad (6-12)$$

So, given the free space two rays attenuation parameters A_{0t} and A_{1t} , and the attenuation due to diffraction A_{0d} , A_{1d} and A_{Ls} , it is possible to compute the weighted

average attenuation in points d_0 , d_1 and d_L as:

$$\begin{aligned} A_o &= wA_{0t} + (1 - w)A_{od}; \\ A_1 &= wA_{1t} + (1 - w)A_{1d}; \\ A_{Ls}. \end{aligned} \tag{6-13}$$

where w is the weighting term defined as:

$$w = (1 + f + \delta h 10^{-4})^{-1} \tag{6-14}$$

For smooth terrain or water, for which δh is lower, the attenuation due to two rays is predominant; for very irregular terrain for which δh is high, also in region 1, the attenuation is mostly due to diffraction phenomena.

The overall attenuation in region 1 can be then calculated (in dB) as :

$$A_{cr} = A_0 + k_1(d - d_0) + k_2 \log\left(\frac{d}{d_0}\right). \tag{6-15}$$

The constants k_1 and k_2 can be set equal to:

$$\begin{aligned} k_2 &= 0; \\ k_1 &= \frac{(A_{Ls} - A_0) - k_2 \log\left(\frac{d_{Ls}}{d_0}\right)}{d_{Ls} - d_0}; \end{aligned} \tag{6-16}$$

If $k_1 < 0$ then:

$$\begin{aligned} k_1 &= 0; \\ k_2 &= \frac{A_{Ls} - A_0}{\log\left(\frac{d_{Ls}}{d_0}\right)}; \end{aligned} \tag{6-17}$$

The diffraction attenuation terms A_{ed} and m_d are, respectively, the intercept and the slope of a line crossing the diffraction attenuation calculated at distances d_3 and d_4 , which are:

$$\begin{aligned} d_3 &= d_L + 0.5\left(\frac{a^2}{f}\right)^{\frac{1}{3}} \quad \text{if } d_3 \leq 0 \text{ then } d_3 = d_{Ls}; \\ d_4 &= d_3 + 0.5\left(\frac{a^2}{f}\right)^{\frac{1}{3}}. \end{aligned} \tag{6-18}$$

The overall diffraction attenuation is then computed as a weighted average between diffraction due to smooth terrain (A_r) and diffraction due to many obstacles (A_k).

In order to compute A_k four parameters are needed:

$$\begin{aligned} v_{1,3} &= 1.2915\theta_3 \sqrt{f \frac{d_{L1}(d_3 - d_L)}{(d_3 - d_{L2})}}; & (6-19) \\ v_{2,3} &= 1.2915\theta_3 \sqrt{f \frac{d_{L2}(d_3 - d_L)}{(d_3 - d_{L1})}}; \\ v_{1,4} &= 1.2915\theta_4 \sqrt{f \frac{d_{L1}(d_4 - d_L)}{(d_4 - d_{L2})}}; \\ v_{2,4} &= 1.2915\theta_4 \sqrt{f \frac{d_{L2}(d_4 - d_L)}{(d_4 - d_{L1})}}. \end{aligned}$$

where:

$$\begin{aligned} \theta_3 &= \theta_e + \frac{d_3}{a}; & (6-20) \\ \theta_4 &= \theta_e + \frac{d_4}{a}. \end{aligned}$$

θ_e is the sum of the elevation angles.

Therefore:

$$A(v_{i,j}) = \begin{cases} 6.02 + 9.11v_{i,j} - 1.27v_{i,j}^2 & \text{for } 0 \leq v_{i,j} \leq 2.4; \\ 12.953 + 20 \log(v_{i,j}) & \text{for } v_{i,j} > 2.4. \end{cases} \quad (6-21)$$

$$A_{k3} = A(v_{1,3}) + A(v_{2,3}), \quad A_{k4} = A(v_{1,4}) + A(v_{2,4}) \quad (6-22)$$

After having computed the attenuation due to smooth terrain in d_3 and d_4 , it is necessary to find the diffraction attenuation in the case of irregular terrain. To that, in annex 3 of [102] there is a set of equation to follow, but in [103] released by the *International Telecommunication Union* (ITU), which is an ONU agency for telecommunication standardization, in addition to the same algebraic method, it is defined a graphical way to compute A_r .

Given:

$$A_r = F(d) + H(h_1) + H(h_2) \quad (6-23)$$

In [103] from Figure 3 to 6, nomograms are provided to compute the values of distance $F(d)$ and the height-gains $H(h)$.

In this way it is possible to obtain:

$$A_{r3} = F(d_3) + H(h_1) + H(h_2), \quad A_{r4} = F(d_4) + H(h_1) + H(h_2) \quad (6-24)$$

Once attenuations due to both smooth terrain and multi-obstacles have been obtained, the averaged attenuations are computed as [102]:

$$\begin{aligned} A_3 &= w_3 A_{r3} + (1 - w_3) A_{k3}; & (6-25) \\ A_4 &= w_4 A_{r4} + (1 - w_4) A_{k4}. \end{aligned}$$

In which the weighting factor w_i is equal to:

$$w_i = \left\{ 1 + 0.1 \left[\frac{\delta h}{\lambda} \left(\sqrt{\frac{h_{e1}h_{e2} + C}{h_{g1}h_{g2} + C}} + \frac{a\theta_e + d_L}{d_i} \right) \right]^{\frac{1}{3}} \right\}^{-1} \quad (6-26)$$

For antenna with known parameters $C = 10$, otherwise $C = 0$.

Having found all the attenuation terms due to diffraction, it is possible to compute A_{ed} and m_d , which are also required in eq. 6-12.

$$m_d = \frac{(A_4 - A_3)}{(d_4 - d_3)}, \quad A_{ed} = A_{f0} + A_4 - m_d d_4. \quad (6-27)$$

The term A_{f0} is defined as a clutter factor, it means that it is useful to take into account all unwanted effects due to echoes. It can be approximated with 15 dB.

Finally it is possible to define the attenuation due to diffraction in region 2 as:

$$A_{cr} = A_{ed} + m_d d. \quad (6-28)$$

Regarding region 3 it is reported as delimiting distance d_x between region 2 and region 3 the approximation:

$$d_x = d_L + 0.25 \left(\frac{a^2}{f} \right)^{\frac{1}{3}} \log f \quad (6-29)$$

Considering $f=868$ MHz, an effective earth radius equal to $\frac{4}{3}$ the effective radius and d_L equal zero; the minimum distance for which attenuation due to scatter phenomena is equal to the one caused by diffraction is at the minimum distance of about 33 km which is much larger than the area considered hereafter and moreover far exceed the LoRa communication range. For this reason the calculation needed for computing attenuation in region 3 will not be reported.

6.1.3 Okumura-Hata Path Loss Model

In [104] an empirical formula, that describe the path loss in an urban environment, has been developed based on measurements in the 1960 Okumura report. In [104] author defined a formula which simplified version is reported to be $A+B \log R$ where A is function of the frequency, B function of the antenna height and R depends on the distance. Some assumption has been done during the formulation of the equation: isotropic antennas are considered and no terrain irregularity have been taken into account.

In Table 3 of [104] the results have been summarized: where:

Area	Path Loss (dB)
Urban	$L_p = 69.55 + 26.16 \log f - 13.82 \log h_t - m(h_r)$
Sub-urban	$L_{ps} = L_p - 2 \left\{ \log \left(\frac{f}{28} \right) \right\}^2 - 5.4$
Open-area	$L_{po} = L_p - 4.78 (\log f)^2 + 18.33 \log f - 40.94$

- f is the carrier frequency in Mhz;
- $m(h_r)$ is a corrective factor depending on the area of interest:

– large city:

$$\begin{aligned} m(h_m) &= 8.29 (\log (1.54h_t))^2 & \text{if } f \leq 200 \text{ MHz;} \\ &= 3.2 (\log (11.75h_t))^2 & \text{if } f \geq 400 \text{ MHz.} \end{aligned}$$

– medium-small city:

$$m(h_m) = (\log (f - 0.7)) h_t - (1.56 \log f - 0.8)$$

- h_r is the transmitter antenna height in meters;
- h_t is the receiver antenna height in meters.

It is also reported that the conditions for which the Okumura-Hata model equations are valid are that: frequency must be in the range 100 MHz - 1500 MHz, distance between transceiver must not exceed 20 km, h_t must be within 30 m - 200 m and h_r within 1 m - 10 m.

6.2 Comparison between Path-Loss Models

In this section will be compared the empirical methods previously introduced. The Longley-Rice method (presented in 6.1.2) requires precise information regarding the terrain curve, so the method is applied on the *Scenario 1* detailed in Section 6.3.1.

In *Scenario 1*, given the transmitter locations, it is possible to define both LOS transmission path and path obstructed by natural obstacles. The two considered transmitters have an omnidirectional antenna with 3dB gain. TX1A is at 10 m from ground while TX1B almost at an height of 30 m from ground.

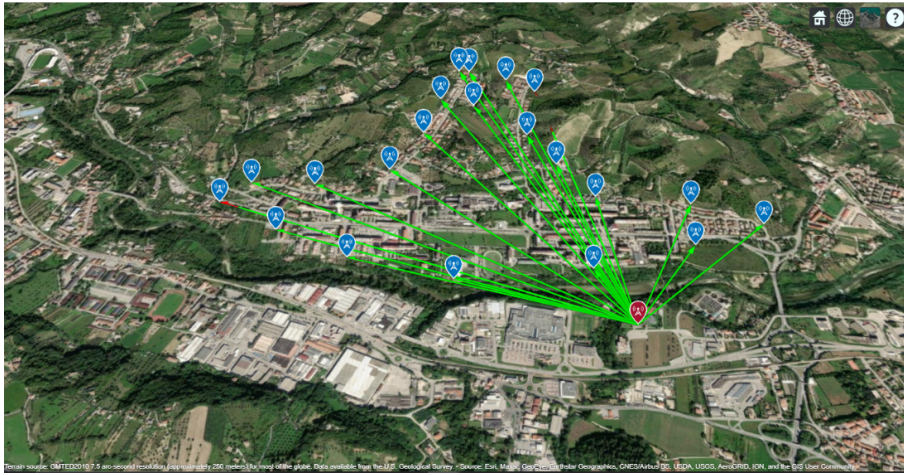


Figure 6.2: Transmission paths for TX1A. Matlab Site Viewer.

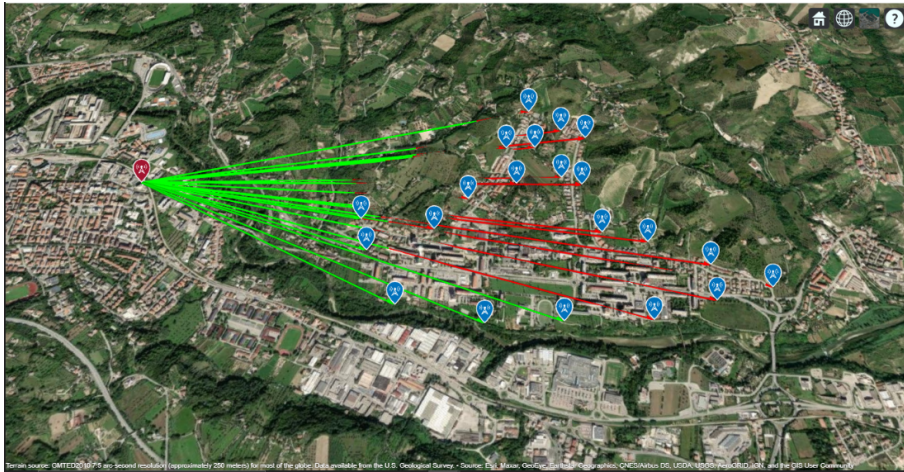


Figure 6.3: Transmission paths for TX1B. Matlab Site Viewer

As it is possible to see, for transmitter TX1A the area of interest is mostly in LOS (Fig. 6.2), that means that for this case the computation of the Longley-Rice attenuation will be under the Region 1 conditions, this means that the two ray attenuation will be mostly considered. Concerning TX1B (Fig. 6.3) the zone of interest is shielded by a hill, but the distance is much lower than the one computed with 6–29; for that reason the Longley-Rice model will consider diffraction attenuation in the way that was explained for Region 2 in Section 6.1.2. The selected paths for TX1A and TX1B are shown in Fig. 6.4 and Fig. 6.5.



Figure 6.4: TX1A LOS path. Matlab Site Viewer.

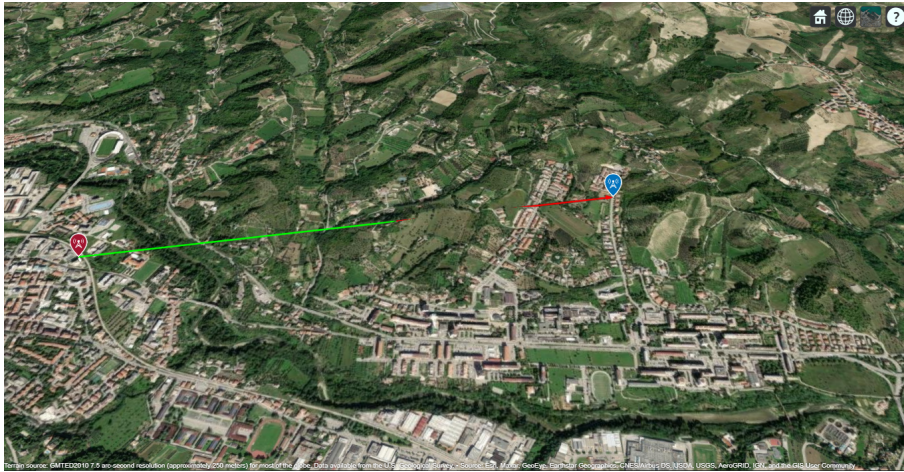


Figure 6.5: TX1B obstructed path. Matlab Site Viewer

The Longley-Rice attenuation curves have been obtained through the *sigstrength* function included in the *MATLAB RF Toolbox* while Free Space Path Loss curve and Okumura-Hata attenuation curves have been obtained using eq.6–2 and equations in section 6.1.3. For the calculation has been considered a transmitter antenna height of 30 m from ground, since it is the lowest acceptable value for the Okumura-Hata method; receiver antenna height has been fixed at 2 m from ground. Frequency has been set equal to 868 MHz. Attenuation is independent from transmitted power and antenna gains.

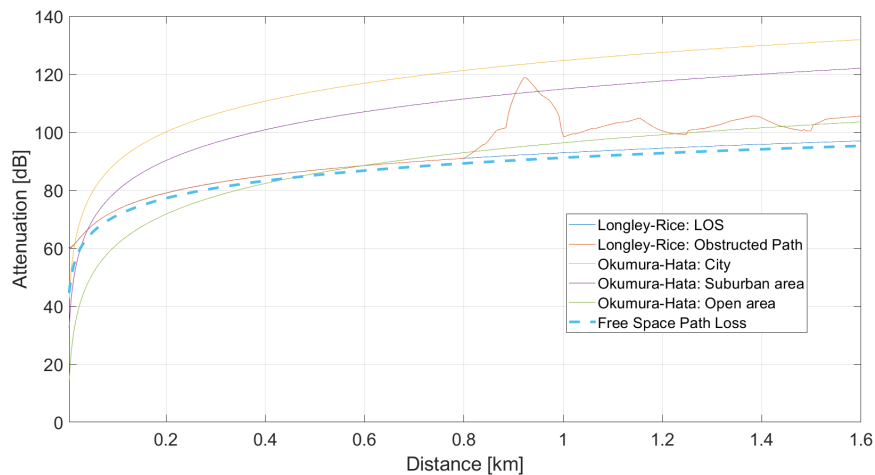


Figure 6.6: Comparison between different empirical models for path loss attenuation.

Table 6.2: Path Loss Methods comparative table for fixed distances.

	5 m	50 m	500 m	1000 m	1500 m
Longley-Rice: LOS	60.0	67.8	86.9	92.9	96.4
Longley-Rice: Obstructed	59.7	67.5	87.0	100.7	102.3
Okumura-Hata: City	43.7	78.9	114.1	124.7	130.9
Okumura-Hata: Suburban	33.8	69.0	104.3	114.9	121.1
Okumura-Hata: Open space	15.3	50.5	85.8	96.4	102.6
Free Space Path Loss	45.2	65.2	85.2	91.2	94.7

The Okumura-Hata method has been applied for a medium-small city, but regarding a big city it is sufficient to add 0.23 dB to the attenuation values. The difference between a big and a medium-small city become more significative when receiver antenna are placed at an higher level.

From Fig. 6.6 can be drawn some observations. For LOS, the Longley-Rice method gives results very similar to the Free Space Path Loss. After 50 m the difference is constant and the LOS Longley-Rice has a worsening of 1.7 dB.

Along the obstructed path, the curve is very similar to the one for the LOS path up to a distance of 800 m where there is a huge attenuation peak. The reason of that can be understood looking at Fig. 6.7.



Figure 6.7: Course of the land along obstructed path and TX1B LOS.

Around 750 m the presence of the hill, that fix the horizon level for TX1B, arise high attenuation due to diffraction, up to 20 dB higher than the Free Space Path Loss Fig. 6.6). After 1 km the values of attenuation become very similar to the ones computed with the Okumura-Hata model for the Open Space. In fact, in open space, the buildings are very few, making the attenuation phenomena similar to the ones considered by the Longley-Rice model for *Region 2*.

Although Okumura-Hata model take into account the effects of buildings, must be noticed that this is a general method and should be fixed for each use-case while

the Longley-Rice model, that only considers attenuation due to terrain, has the advantage of consider local parameters, such as the coordinates, altitude but also the refractivity index which in turn depend on annual variation based on the weather of a zone.

6.3 Simulation

In this section will be carried out a simulation on *Scenario 1* and *Scenario 2*, described in section 6.3.1, in order to evaluate the coverage of transceivers based on a LoRa module. Transmitter and receiver have been modelled following the parameters of the TTGO LoRa32 board supporting the SX1276 868MHz LoRa module. For this module the maximum TX power is equal to 20dBm and has a maximum sensitivity of -148 dBm. The working frequency is 868 MHz and the antenna considered is a quarter wavelength monopole wire. Considering also a velocity factor of 95% the final antenna length is 8.2 cm.

Height of transmitter and working frequency have been kept fixed while height of receivers and output power values have been swept in order to find the best compromises that gave the complete coverage. It is clear that the simulation has to be intended only as a preliminary tool just to get an idea about the feasibility of the LoRa communication in the considered sites.

Looking at Fig. 6.6 it is possible to see that there are about 35 dB of difference between the LOS Longley-Rice attenuation curve and the Okumura-Hata attenuation curve in city environment; for this reason, and eventually to consider further diffraction phenomena, during the simulation the coverage has been considered acceptable only for a received signal power higher than -90 dBm although the RF transceivers supported by the TTGO LORA32 board has a sensitivity of -148dBm.

The simulation has been done with *MATLAB* and mostly by means of the *RF Toolbox*. The RF Toolbox take into account the Longley-Rice Path Loss Model to compute the attenuation.

6.3.1 Scenarios

From hereafter there will be considered two scenarios for the application of the Path Loss models previously presented. The first scenario (*Scenario 1*) in Fig. 6.8 is a neighbourhood in a medium city. The zone is mostly plain with surrounding hilly reliefs. A LoRa WSN has to be installed in this neighbourhood with two transmitting stations (TX1A and TX1B) that are wanted to cover the area. TX1A is at the south of this area while TX1B is at the west. TX1A is placed on a building with an height of 10 m, while TX1B is on the roof of a six floors building with an overall height

of 30 m. Five observation points (RX1, RX2, RX3, RX4, RX5) have been chosen to characterize the neighbourhood. Considering the neighbourhood borders, maximum distance from TX1A is about 1.6 km, while TX1B is more than 3 km away from the farthest east point belonging to the neighbourhood.

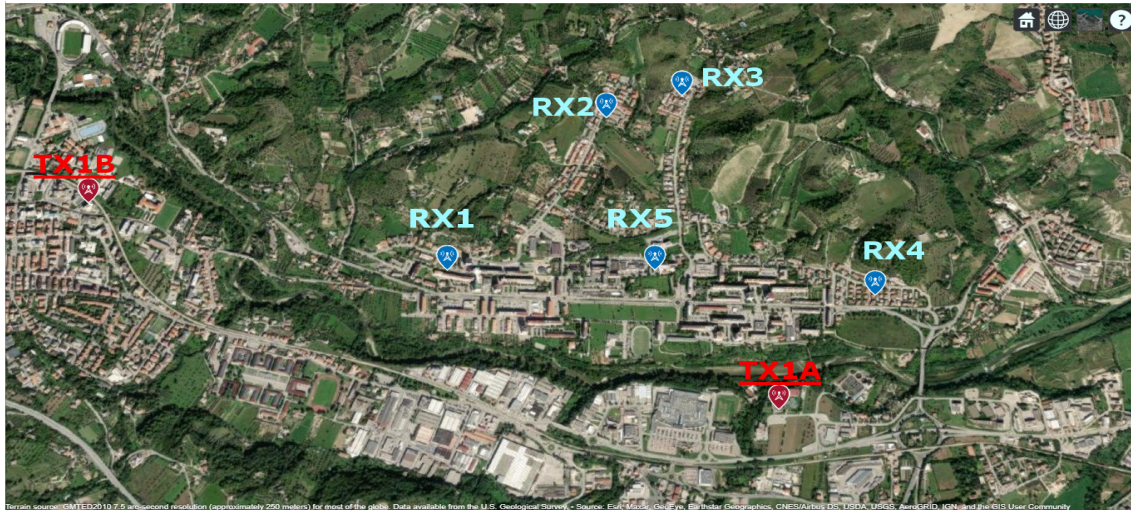


Figure 6.8: *Scenario 1*: Map showing location of Monticelli neighbourhood (AP). Matlab Site Viewer



Figure 6.9: *Scenario 2*: Map showing a maritime zone (AP). Matlab Site Viewer

The second scenario (*Scenario 2*) is a maritime zone, depicted in Fig. 7.1. Communication must be ensured along the coast, in particular two residential area (around RX1 and RX2 in figure 7.1) are required to be supplied with coverage. Also in this case two transmitter stations (TX2A and TX2B) have been considered. TX2A, that is used to irradiates the area around RX1 which is 1.6 km far, is placed on a hill quite higher than the coast. TX2B is mostly at the sea level and should cover the area around RX2 that is about 1.5 km far.

6.3.2 Results

Scenario 1

At first it has been plotted the coverage for the single antennas for different output power and receiver heights of 1 m.

In this way it has been possible to see that TX1B, also with the maximum output power of 20 dBm could not manage to supply RX2, RX3, RX4 and RX5 with a signal strength higher than -90 dBm (Fig.6.11). This is due to the presence of an hill fencing good part of the zone of interest from TX1B. Since TX1B could only cover the area around RX1, an output power of 11 dBm would be sufficient (Fig. 6.11).

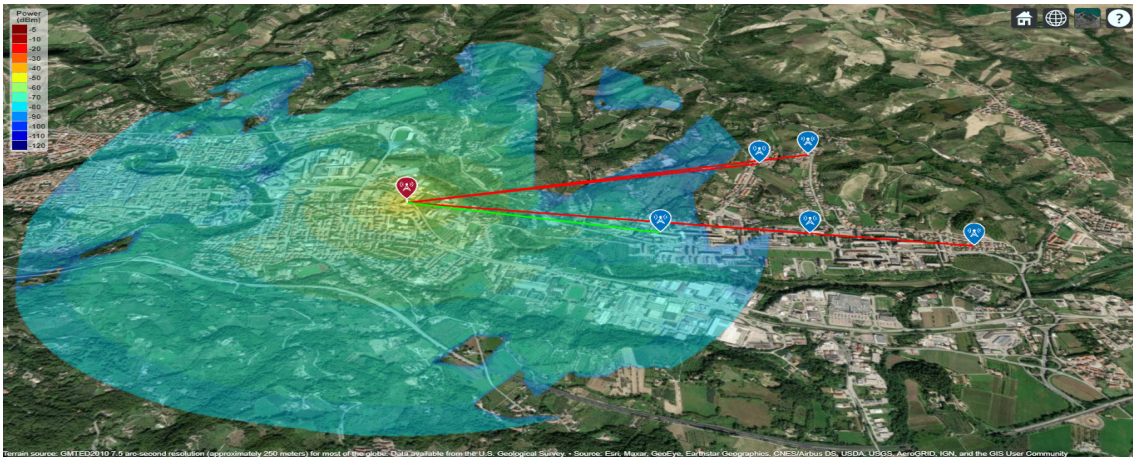


Figure 6.10: *Scenario 1*: TX1B, Output Power: 20 dBm, Receivers Height: 1 m

Considering TX1A, with transmitter power 20 dBm and receiver height 1 m, the *Scenario 1* is mostly covered in its entirety, except for an area around RX3. With the maximum output power there is also a large amount of signal in unwanted directions. It has been seen that RX3 receive a signal higher than -90dBm only for receivers height of 8 m. For that receivers height, RX3 is supplied also with an output power of 11 dBm receiving -85 dBm (Fig. 6.12).

The area around RX3 would receive an acceptable power only for receiver placed higher than 8 m, independent from the output power of TX1A while TX1B would not reach that point for any configuration of power and height. For this reason, a good compromise, would be to use transmitter output power of 11 dBm, keeping the receivers at 1 m, in this way the installation would be easier, but for the area around RX3 the receivers should be placed at least at 8 m. With this configuration the coverage depicted in figure 6.13 has been obtained.

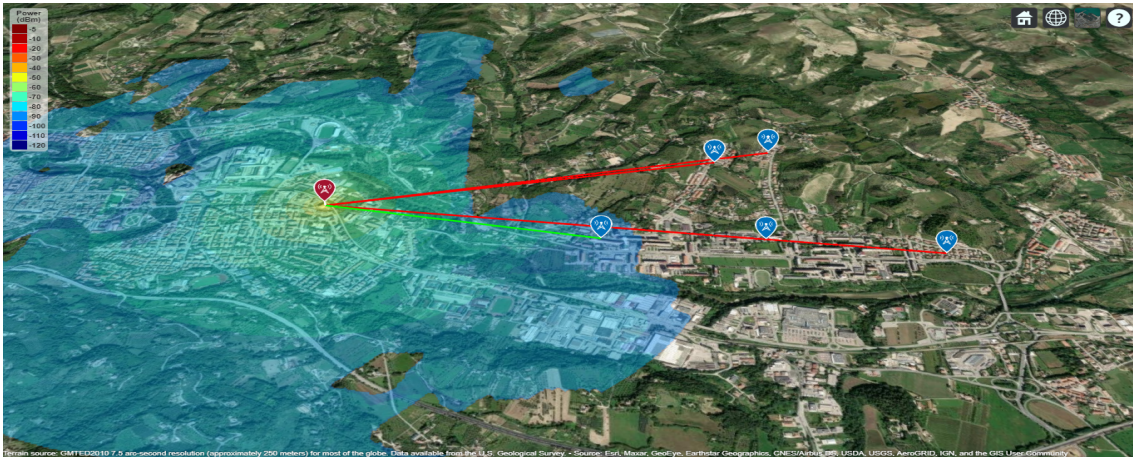


Figure 6.11: *Scenario 1*: TX1B, Output Power: 11 dBm, Receivers Height: 1 m

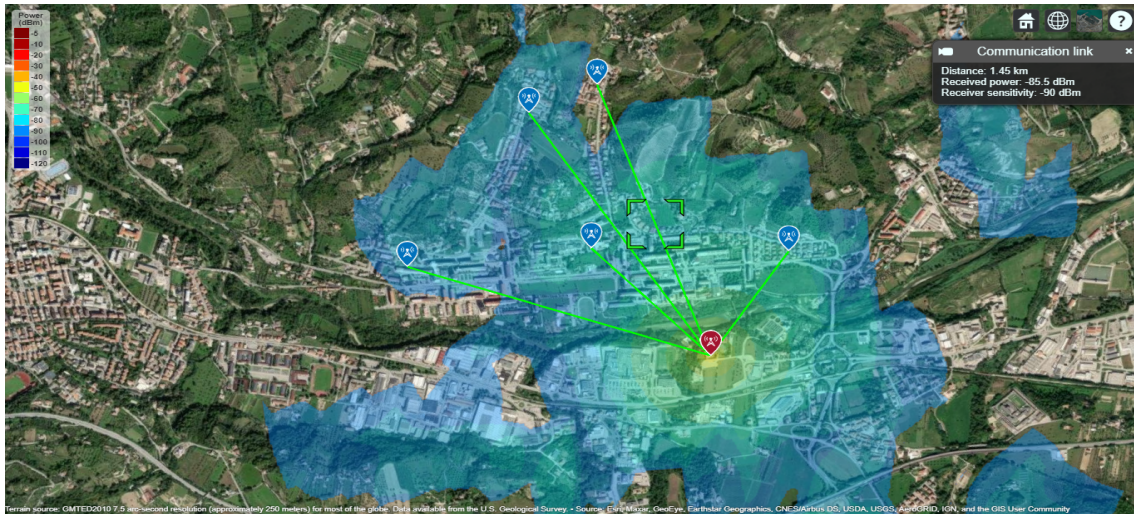


Figure 6.12: *Scenario 1*: TX1A, Output Power: 11 dBm, Receivers Height: 1 m, 8m for RX3.

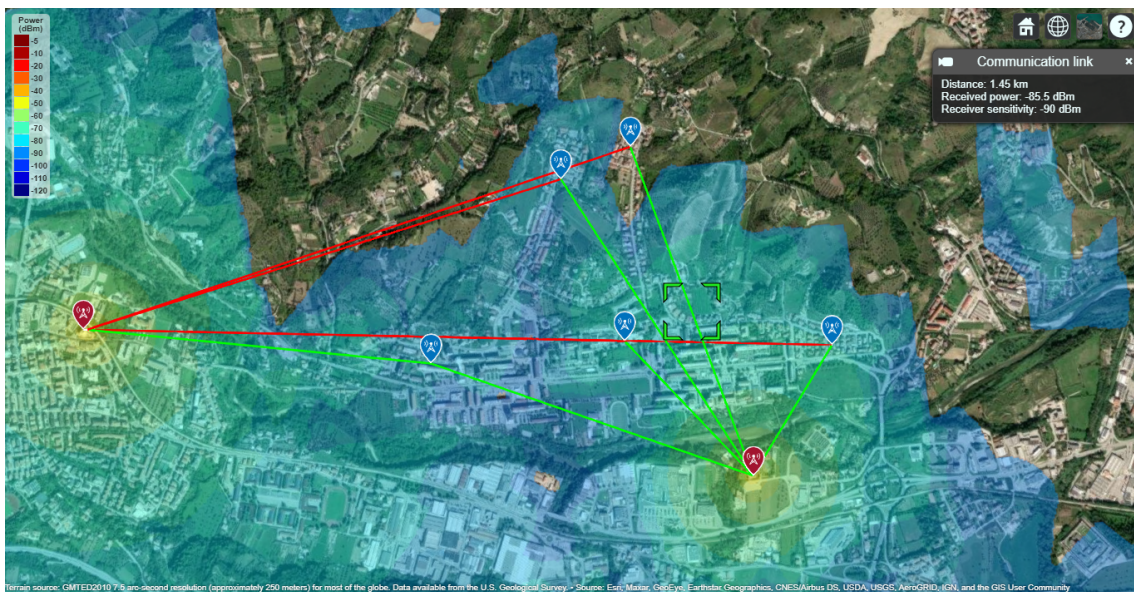


Figure 6.13: *Scenario 1*: TX1A & TX1B, Output Power: 11 dBm, Receivers Height: 1 m, 8m for RX3.

Scenario 2

For the *Scenario 2* have been provided two transmitters: TX2A that is on a hill and TX2B which is at the sea level. The aim is to understand if this two transmitter

could cover the coast area, especially the two residential area that are marked as RX1 and RX2 in Fig. 7.1.

The simulation has been conducted for transmitter power equal to 11, 14 and 20 dBm. For each power level receivers antenna height of 1, 4, 8 m have been tested. Focusing on TX2A at first, it has been possible to see that increasing both the output power and the receivers antenna height no significant improvement could have been obtained in the covered range toward the north. This is due to the presence of a relief that cause major attenuation in that direction. Moreover increasing the output power great part of signal is spread in the hinterland and over the sea, which are out of the zone of interest. With an output power of 11 dBm the receiver height around RX1 are required to be higher than 8 m to assure coverage along the coast. Using 14 dBm, with an height of 4 m, the same results can be obtained compared to the previous case (Fig. 6.14 and Fig. 6.14).

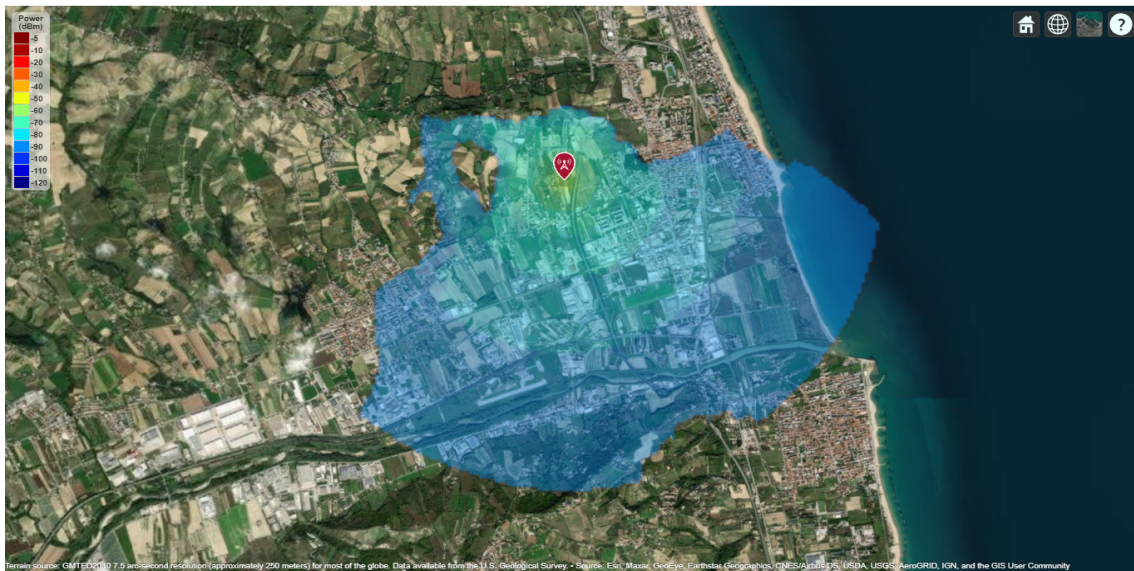


Figure 6.14: *Scenario 2*: TX2A, Output Power: 11 dBm, Receivers Height: 10 m.

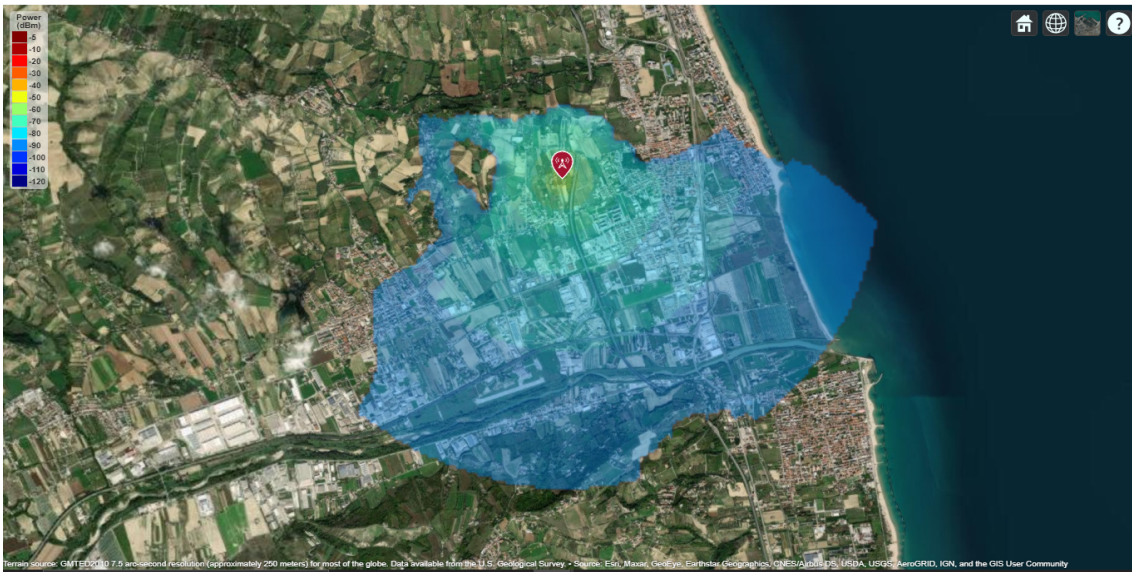


Figure 6.15: *Scenario 2*: TX2A, Output Power: 14 dBm, Receivers Height: 4 m.

Regarding TX2B the residential area around RX2 would receive a good signal in two cases: for output power equal to 11 dBm and receivers antenna height of 8 m (Fig. 6.16), or with output power equal to 14 dBm and receivers height of 4 m (Fig. 6.17).



Figure 6.16: *Scenario 2*: TX2B, Output Power: 11 dBm, Receivers Height: 8 m.

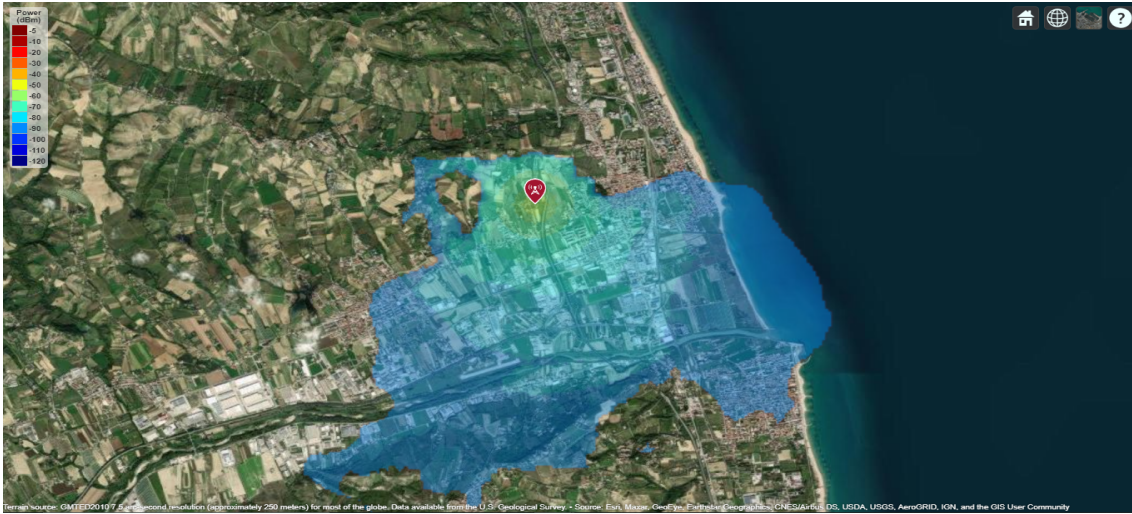


Figure 6.17: *Scenario 2*: TX2B, Output Power: 14 dBm, Receivers Height: 4 m.

The total area belonging to the *Scenario 2* would be supplied with a good signal coverage using both transmitter with an output power of 14 dBm and setting the receivers antenna height to 4 m. The area would also be covered by a single antenna with 20 dBm of output power, but the receiver height should be 4 m also in this case and there would be great part of transmitted power on unwanted zones (Fig. 6.18).



(a) TX2A & TX2B, Output Power: 14 dBm, Receivers Height: 4 m.



(b) TX2A, Output Power: 20 dBm, Receivers Height: 4 m.

Figure 6.18: *Scenario 2: Coverage of Scenario 2.*

6.3.3 Final Observation

In Section 6.2 it was noticed that the attenuation computed with the empirical Okumura-Hata path loss model is, in general, higher than the one predicted by the Longley-Rice model. In particular, the Okumura-Hata attenuation in a city exceeded by almost 35 dB the attenuation computed with the Longley-Rice model along the LOS path considered. Nevertheless, the Longley-Rice model takes into account local parameters, as described in Section 6.1.2. During the simulation it has been considered for the received signal an acceptable strength equal or higher than -90 dBm in order to keep in consideration attenuation phenomena not included in the Longley-Rice method. After these considerations, the parameters of the TTGO LoRa32 have been taken into consideration. Aim of the simulation in Section 6.3.2 was to find a trade-off between output power and receivers antenna height to overcome the terrain obstruction in the two area considered (Section 6.3.1).

According to the simulation, the *Scenario 1* could be properly covered by the signal using a power output of 11 dBm for both transmitter when the receivers were placed at 1 m from ground. Keeping reducing the power, the height of the receivers should be increased making installation of an eventual WSN more difficult. Around RX3 in Fig. 6.8 the receiver height required should be around 8 m since it is just behind an hill. The terrain attenuation could not have been overcome with lower receivers height also with the maximum output power of 20 dBm. In *Scenario 2* two transmitter have been placed to cover two residential areas. Again the terrain conformation has huge impact, in particular for TX2A in Fig. 7.1 an hill completely shielded the signal toward north. Residential areas around RX1 and RX2 have been completely covered using an output power of 14 dBm for both transmitters and a receivers height of 4 m. The *Scenario 2* could have been supplied with good signal also with only one transmitter exploiting 20 dBm output power, but in this way there would also have been a waste of radiated power in areas outside the zone of interest (Fig. 6.18).

The coverage in *Scenario 1* would be possible with less power and lower receivers height since the neighbourhood is on an uphill plain, and for this reason it is mostly LOS with TX1A; in *Scenario 2* the two residential areas are further from transmitter with respect to *Scenario 1* and all the zone to be irradiated is at sea level, making the ground reflection more significant.

Chapter 7

Measurements

In Chapter 6 it was seen that the Longley-Rice model is good for determining whether the terrain in the area under interest presents impairment for the communication for a given transmitter. If not, it is better to rely on models that take into account further diffraction phenomena due to buildings, for example the Okumura-Hata model. Nevertheless, each case study is different and could differ from empirical models.

In this section it will be conducted some measurements in a sub-urban environment to characterize the LoRa path loss behaviour and to see if and how it differs from proposed models. Case studies cover both indoor and outdoor scenarios. The measurements set-up involves two TTGO LoRa32 boards where an ESP32 and a Semtech SX1276 chip are mounted. One board has been configured as transmitter, the other one as receiver with the Arduino IDE. The ESP32 offers the possibility to measure the RSSI, this functionality has been used to map the path loss of the LoRa communication.

For the outdoor transmission the LoRa parameters have been set in order to achieve maximum distance, while for the indoor case it has been tried to use the lowest power needed to cover the area under interest. For both the cases the center frequency of 868 MHz has been used, for which, according to the Italian law [105], a duty cycle of 1% must be respected; this means that only 36 seconds per hour are allowed for transmission. The length of the payload also affects the time on air.

After the measures have been recorded, a linear regression fit algorithm has been implemented in order to find a log-distance model [24]:

$$L_p = \beta_1 + 10\beta_2 \log(d) + X \quad (7-1)$$

where:

- L_p is the path loss in dB;

- β_1 and $10\beta_2$ are the output of the linear regression fit method, which are respectively the intercept and β_2 is the distance power loss factor;
- X is a random variable.

The X random variable is used to probabilistically characterize the effects of multipath and shadowing interferences. According to the theory [106, 107], when the power samples are taken on channel that vary spatially more than 10λ (λ is the wavelength) the transmission is affected by shadowing (slow fading) and X is expected to be log-normally distributed. X_i will be computed as:

$$X_i = L_{p_m}(d_i) - L_p(d_i) \quad (7-2)$$

where:

- $L_{p_m}(d_i)$ is the measured path loss at the distance d_i ;
- $L_p(d_i)$ is the path loss computed with: $\beta_1 + 10\beta_2 \log(d_i)$.

For both the indoor and outdoor cases (since for the central frequency of 868 MHz, λ is equal to 34 cm and so the overall distances are higher than 10λ), the X_i samples are expected to be normally distributed in logarithmic scale with a standard deviation of X_σ .

7.1 Results for outdoor path loss

Table 7.1: LoRa parameters set-up for outdoor communication.

Tx Power	20 dBm
Antenna gain	2.15
BW	125 kHz
Center Freq.	868 MHz
SF	12
CR	4/5
Time on Air	827.39 ms
Transmitter height	4 m

In order to achieve the maximum distance for the communication, it has been used an output power of 20 dBm and a spreading factor of 12, which would increase the sensitivity according to the documentation [108]. The transmitter has been positioned at 4 m height from ground while the receiver was hand-held. The antenna is omnidirectional with a directivity of 2.15 dB. With these parameters the scripts implemented for the Chapter 6 have been used for carrying out a first simulation exploiting the Longley-Rice model. The resulting coverage is depicted in Fig. 7.1.



Figure 7.1: Coverage accordingly to Longley-Rice

Without considering the attenuation caused by buildings, the area of interest would be covered since no terrain obstruction are presents, but once this is ascertained, since the antenna is in an urban area, from now on the Okumura-Hata will be used as comparison with the measured attenuation, given that this model consider further attenuation phenomena, as seen in Chapter 6.

In order to respect the 1% duty cycle limitation only 1 packet every 1mm:23ss has been sent for a total of 107 samples. The points where the RSSI have been recorded have been signed on the map reported in Fig. 7.2.

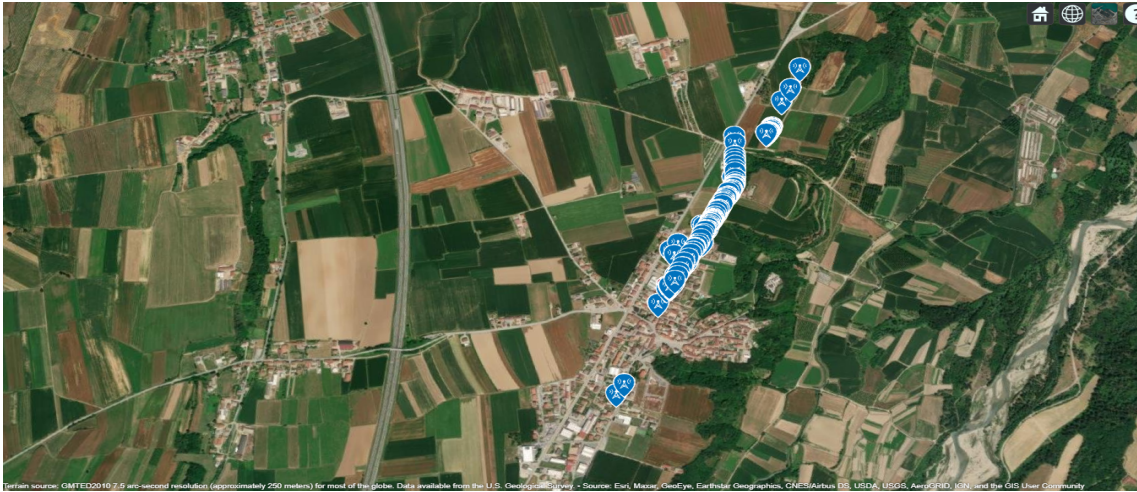


Figure 7.2: Receiving points

Following there are the results of measured attenuation in comparison with the Okumura-Hata path loss curves (Fig. 7.3)

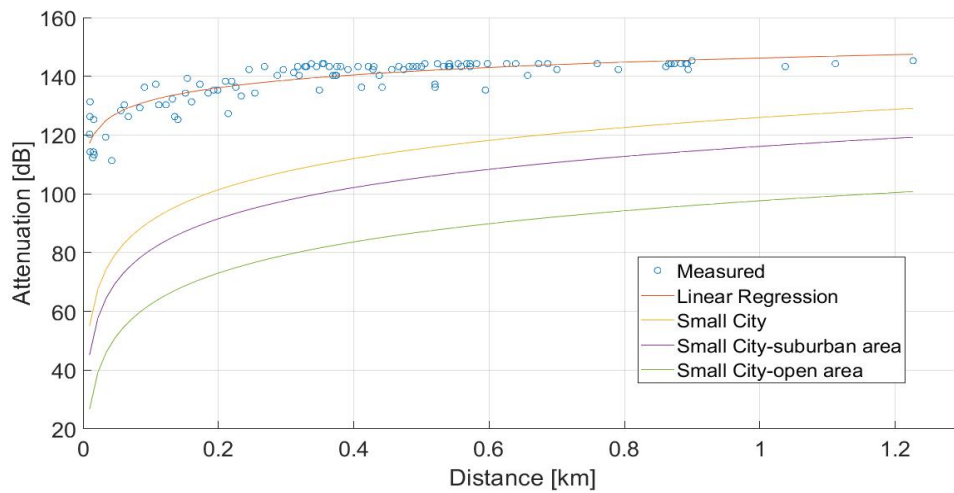


Figure 7.3: Outdoor Path Loss

It is possible to see that in the sub-urban environment considered, the maximum range that has been possible to obtain is of about 1.3 km, but only up to 600 m the packets have been received continuously. Until the distance of 500 m the transmitter and receiver have been in LOS.

In Fig. 7.4 it has been plotted the cumulative distribution function of the deviation of the measured samples from the predicted ones (X), which have zero mean and

standard deviation $X_\sigma = 3.95$. For comparison in Fig. 7.4 has been also plotted the CDF of a normal distributed variable with same mean and standard variation as the samples. It is possible to see that the empirical CDF follows the CDF of a normal distribution with zero mean and standard deviation equal as the one computed from the samples.

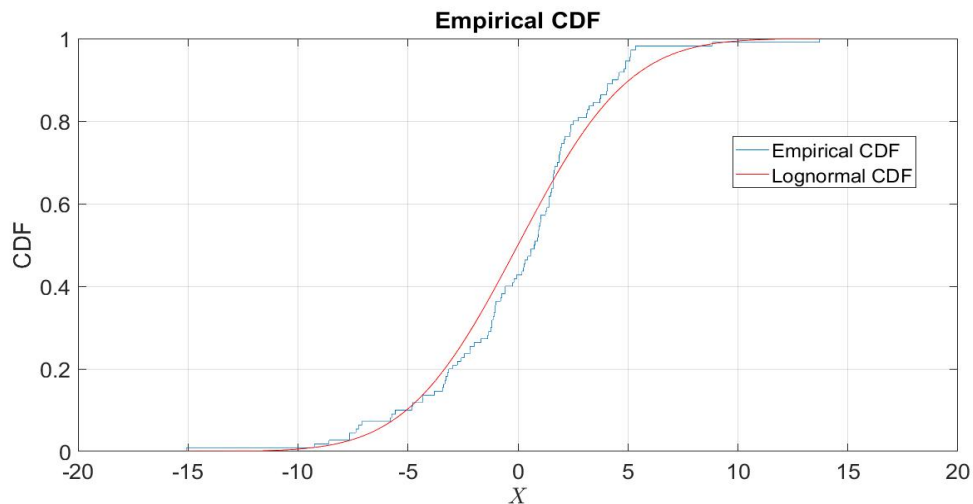


Figure 7.4: CDF of the deviation from predicted attenuation value (in dB)

The path loss prediction model that has been obtained for the sub-urban environment under consideration is:

$$L_p = 146.21 + 14.4 \log(d) + X \quad (7-3)$$

7.2 Results for indoor path loss

Table 7.2: LoRa parameters set-up for indoor communication.

Tx Power	11 dBm
Antenna gain	2.15
BW	125 kHz
Center Freq.	868 MHz
SF	7
CR	4/5
Time on Air	30.98 ms
Transmitter height	1.10 m

At first a general investigation has been conducted over the indoor (domestic) area under study in order to find the lowest value of power needed, resulting in 11 dBm (Fig. 7.5).

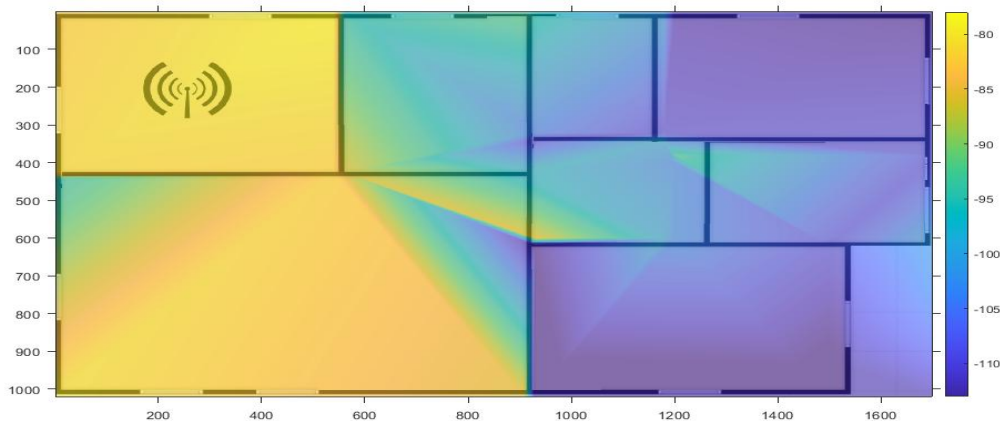


Figure 7.5: Coverage of the indoor area

A SF of 7 has been chosen since the requirements on distance where no longer needed and in this way the time on air has been significantly reduced. That allowed to transmit a packet every 3 seconds and 1800 samples have been taken for the LOS case. In indoor set-up measurements have been taken for LOS transmitter and receiver over the same floor and also in the case for which there was a floors of difference between the two. Keeping the receiver fixed in the same position at the ground floor a hundred samples have been taken each meters on a path 17 m long for the LOS case. For the NLOS cases, following the same path as the LOS, but one floor under, 890 samples have been taken .

This time the path loss models presented in Chapter 5 were no longer suitable. For comparison it has been taken the ITU-R indoor model [109].

LOS case

In this case transmitter and receiver have been taken in LOS on the same floor in a residential building. The resulting path loss curve is plotted in Fig. 7.6.

Due to the larger amount of data it is now possible to see in Fig. 7.7 that the CDF of X , with $X_\sigma = 3.21$, better follows the reference normal CDF with same standard deviation.

The final log distance path loss model that has been obtained is:

$$L_p = 87.03 + 24.9 \log(d) + X \quad (7-4)$$

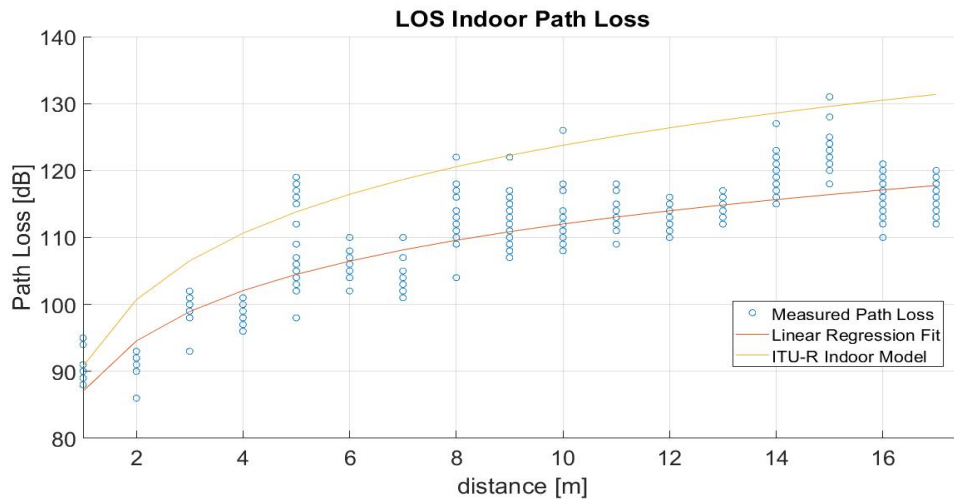


Figure 7.6: Indoor path loss (LOS).

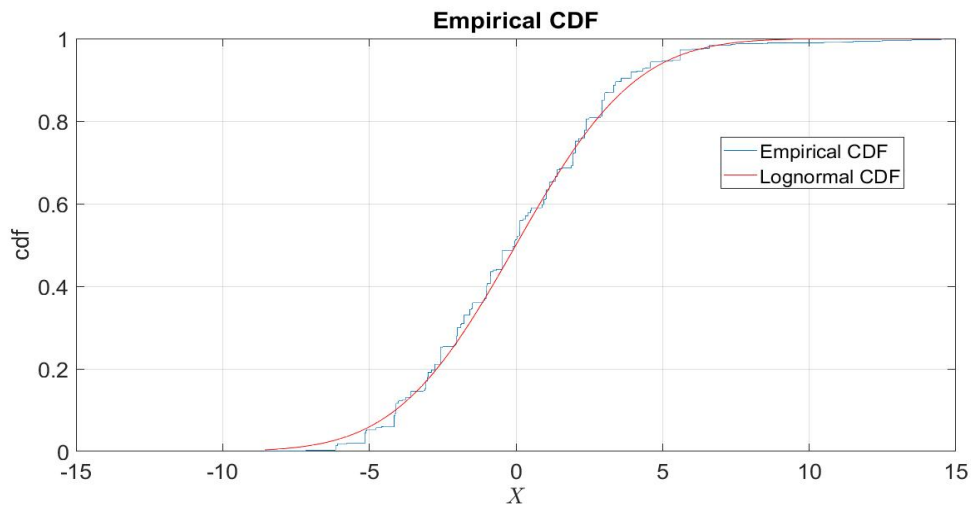


Figure 7.7: CDF of the deviation from predicted attenuation value, in dB (LOS).

NLOS case

In this case measures have been taken one floor under the transmitter, in an underground garage. According to the ITU there should be a worsening of 9 dB with respect to the LOS case [109].

In the considered case the intercept is almost 10 dB higher than the LOS case, this is coherent with what was expected according to the ITU model. The

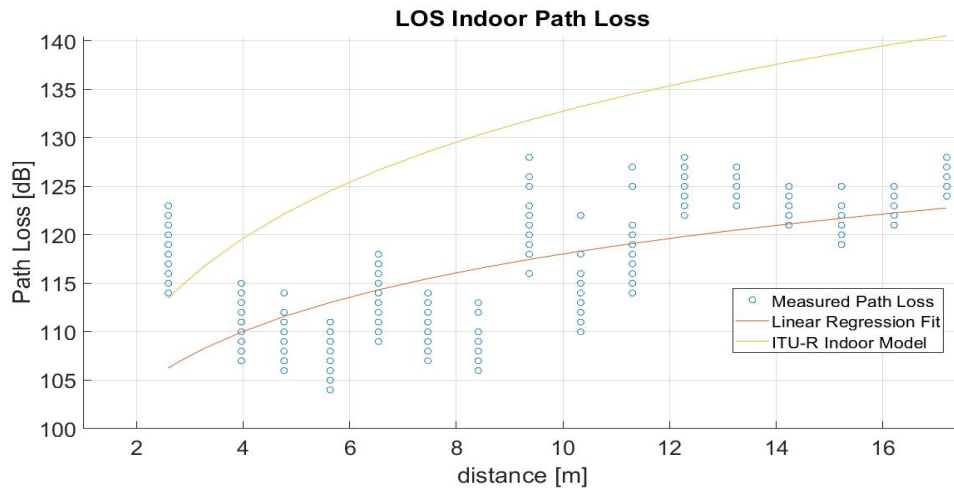


Figure 7.8: Indoor path loss (NLOS).

final log distance model that has been found is:

$$L_p = 97.92 + 20.1 \log(d) + X \quad (7-5)$$

Again, X can be considered to be log-normally distributed, looking at Fig. 7.9. X for the indoor NLOS case has zero mean and $X_\sigma = 4.91$.

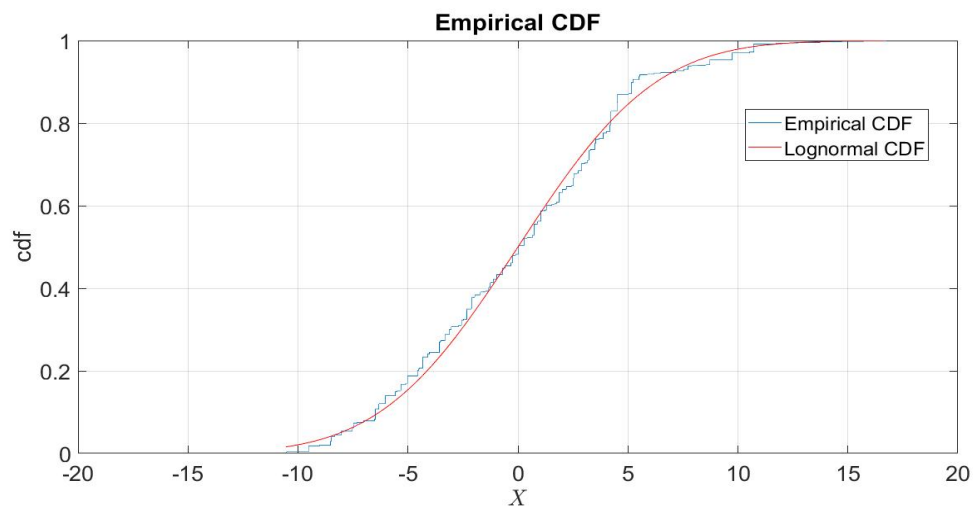


Figure 7.9: CDF of the deviation from predicted attenuation value, in dB (NLOS)

Table 7.3: Comparative table for LOS and NLOS models.

	β_1	β_2	X_σ
LOS	87.03	2.49	3.21
NLOS	97.92	2.01	4.91

7.3 Final Observation

Outdoor case

The maximum recorded distance, with SF equal to 12 and output power of 20 dBm, has been of about 1.3 km, but the packets have been received continuously only up to 500 m. This could be probably due to imperfections in antennas design and in the non optimal transmitter location. Improvements could be achieved increasing the transmitter height and reducing the bandwidth, but this will lead to a further reduction in bit rate and in a consequently increasing in time on air, meaning that less packet could be transmitted per hour according to the 1% duty cycle regulation in the 868 MHz band.

The measured path loss seems to suffer from high attenuation with respect to the Okumura-Hata models, but the recorded data are coherent with the ones in literature [110, 111]. In fact authors of [110] experienced 30 dB difference between the Okumura-Hata model and the measured attenuation, the same as the path loss measured represented in Fig. 7.3.

Moreover authors of [111] found a log distance model for outdoor LoRa communication which are reasonably comparable with the ones proposed:

	β_1	β_2	X_σ
Proposed	146.21	1.44	3.95
[111]	132.25	2.65	-

Indoor case

Indoor transmission, with SF equal to 7 and output power of 11 dBm, achieve good results for both LOS and NLOS cases, regarding the area of interest, with less attenuation with respect to the general empirical path loss model presented in [109]. Difference that have been found within the LOS and NLOS path loss models that have been obtained are coherent with what was described in the ITU model [109]. NLOS intercept and X_σ increase due to floor obstruction and shadowing, while the power loss coefficient remains nearly the same.

Moreover, it has been possible to find that authors of [92] and [112] verified the LoRa

communication defining log distance path loss models, both for LOS and NLOS cases. For comparison in the following table have been reported the values found during this work and in papers review:

	β_1	β_2	X_σ
Proposed (averaged)	92.48	2.25	4.06
[92] (averaged)	40.93	3.30	5.08
[112] (averaged)	125.4	2.85	-

Conclusions

In this work has been firstly presented a comprehensive review on LoRa communication technology in many fields, which have been divided into seven macro areas. A total of fifty-nine papers that deal with LoRa application have been considered. Taking into account the numbers of paper for each area, it is possible to see that the trends in LoRa employment are going towards smart city applications. For this area fourteen papers have been considered. Different studies experienced a communication range of kilometres, assuring high packet reception successful rate. Only with one gateway it could be possible to reach 1km or more. Also, in indoor environment, a gateway could send data to different floors. This means that the LoRa technology is suitable for WSN in urban environment, in particular for static nodes. Following there are healthcare and environmental monitoring application, regarding the number of paper considered. Again these applications are usually fit in an urban context. For all these use-case the data rate has not been a problem since monitored parameter didn't change frequently and the communication usually is event-driven. In this way batteries supplied node can last years. In cities, where vehicles usually have low velocity, LoRa networks could be also used in tracking them. The low data rate of the LoRa communication, which is suitable in mostly urban context, could be a problem in disaster prevention. Although there are papers presenting working systems with LoRa communication, cases where ultra low latency and continuous monitoring are needed for immediate intervention are not compatible with LoRa characteristics for which low power and range are the main objectives. Moreover, in agriculture application, it has been seen that placing nodes under ground deeply worsen communication. Interesting case is the last application presented regarding satellites communication, which is still under study but it seems to have future applications in applications in providing connection in remote areas.

In the second part of the thesis a simulation has been presented over two residential areas. During the simulation an attempt was made to find the best compromise between the output power and the height of the receivers antennas. This two aspect have been taken into account since the low power and the ease of installation are peculiar for a good LPWAN network for the IoT. Moreover it has been possible to

observe that the surrounding land conformation has an huge impact over attenuation. When hills shield the signal in some direction best results have been found in increasing antenna height instead of rising output power. Although these problems, according to the simulation, satisfactory trade-off have been found that could properly provide the areas under interest with a good signal coverage.

In the last part several measurement have been taken in a sub-urban area in order to define a path loss model both for outdoor and indoor applications. For the outdoor scenario the results are not so excellent as expected, but this could be possibly due to impairment during the set-up and better performances could be achieved positioning transmitter at an higher location or choosing antennas with higher gain. Nevertheless, it have been found results in literature that are coherent with the path loss measured during this work. Moreover it has been possible to notice how different could be a general path loss model compared with measurements, but general model could be used to make a preliminary study, in particular the Longely-Rice model is useful to verify if the terrain presents obstruction for a given transmitter. Regarding the indoor measurements, it has been possible to see that a LoRa WSN could suitably cover different floors, experiencing lower attenuation than the general path loss model for indoor applications proposed by the ITU. The values that have been found for the path loss models are similar to the one that can be found in literature. In the indoor scenario analysed here minimum values of SF and power have been exploited, increasing them a WSN in bigger buildings could probably be installed with good performances.

References

- [1] Harald Edquist, Peter Goodridge, and Jonathan Haskel. “The Internet of Things and economic growth in a panel of countries”. In: *Economics of Innovation and New Technology* (2019), pp. 1–22. ISSN: 1043-8599. URL: <https://www.tandfonline.com/doi/full/10.1080/10438599.2019.1695941>.
- [2] *Annual reports archive - Ericsson*. URL: <https://www.ericsson.com/en/investors/financial-reports/annual-reports> (visited on 06/01/2020).
- [3] James Manyika et al. *The Internet of things - Mapping the value beyond the hype*. 2015.
- [4] *Economic impact of the COVID-19 pandemic - Wikipedia*. URL: https://en.wikipedia.org/wiki/Economic_impact_of_the_COVID-19_pandemic (visited on 06/03/2020).
- [5] *Is there a link between IoT and productivity growth? - Ericsson*. URL: <https://www.ericsson.com/en/blog/2020/5/link-between-iot-productivity-growth> (visited on 06/01/2020).
- [6] *Total factor productivity - Wikipedia*. URL: https://it.wikipedia.org/wiki/Total_factor_productivity (visited on 06/03/2020).
- [7] Timothy Malche and Priti Maheshwary. “Internet of Things (IoT) for building smart home system”. In: *Proceedings of the International Conference on IoT in Social, Mobile, Analytics and Cloud, I-SMAC 2017*. Institute of Electrical and Electronics Engineers Inc., 2017, pp. 65–70. ISBN: 9781509032433.
- [8] *Consumers and sustainability report - Ericsson*. URL: <https://www.ericsson.com/en/news/2020/5/consumers-and-sustainability-report> (visited on 06/01/2020).

-
- [9] *IPCC, 2014: Climate Change 2014: Synthesis Report. Contribution of Working Groups I, II and III to the Fifth Assessment Report of the Intergovernmental Panel on Climate Change [Core Writing Team, R.K. Pachauri and L.A. Meyer (eds.)]. IPCC, Geneva, Switzer. Tech. rep. 2014, p. 151.*
- [10] Jens Malmmodin and Pernilla Bergmark. “Exploring the effect of ICT solutions on GHG emissions in 2030”. In: Atlantis Press, 2015.
- [11] *Scania is reshaping the factory of the future - Ericsson.* URL: <https://www.ericsson.com/en/blog/2020/5/scania-factory-of-the-future>.
- [12] Ahmed Elhamy Mostafa, Yong Zhou, and Vincent W.S. Wong. “Connection Density Maximization of Narrowband IoT Systems with NOMA”. In: *IEEE Transactions on Wireless Communications*. Vol. 18. 10. Institute of Electrical and Electronics Engineers Inc., 2019, pp. 4708–4722. URL: <https://ieeexplore-ieee-org.ezproxy.biblio.polito.it/document/8764608>.
- [13] *Cellular networks for Massive IoT/Whitepaper - Ericsson.* URL: <https://www.ericsson.com/en/reports-and-papers/white-papers/cellular-networks-for-massive-iot--enabling-low-power-wide-area-applications> (visited on 06/01/2020).
- [14] *Why LoRa? / Semtech LoRa Technology / Semtech.* URL: <https://www.semtech.com/lora/why-lora> (visited on 06/05/2020).
- [15] L. Carosso, L. Mattiauda, and M. Allegretti. “A Survey on Devices Exploiting LoRa Communication”. In: *Acta Marisiensis. Seria Technologica* 18.2 (2020), pp. 31–35. ISSN: 2668-4217.
- [16] *Semtech.* URL: <https://www.semtech.com/search/results?keywords=modulationbasics{\%}2A> (visited on 07/02/2020).
- [17] Caijiao Xue. “Anti-interference performance of mUlti-path direct sequence spread spectrum wireless communication system”. In: *2010 International Conference on E-Health Networking, Digital Ecosystems and Technologies, EDT 2010*. Vol. 1. 2010, pp. 461–464. ISBN: 9781424455157.
- [18] Juan M. Velazquez-Gutierrez and Cesar Vargas-Rosales. “Sequence Sets in Wireless Communication Systems: A Survey”. In: *IEEE Communications Surveys & Tutorials* 19.2 (2017), pp. 1225–1248. ISSN: 1553-877X. URL: <http://ieeexplore.ieee.org/document/7782831/>.

- [19] Harish Laxmichand Sharma, Atul R. Deshmukh, and N. G. Bawane. “Spread spectrum pattern & PN sequence retrieval in wireless ad hoc network: Design approach”. In: *Proceedings - 2nd International Conference on Emerging Applications of Information Technology, EAIT 2011*. 2011, pp. 391–394. ISBN: 9780769543291.
- [20] Raymond L. Pickholtz, Donald L. Schilling, and Laurence B. Milstein. *Revisions to “Theory of Spread-Spectrum Communications— Tutorial”*. 1984.
- [21] Esmael H. Dinan and Bijan Jabbari. “Spreading codes for direct sequence CDMA and wideband CDMA cellular networks”. In: *IEEE Communications Magazine* 36.9 (1998), pp. 48–54. ISSN: 01636804.
- [22] K. Ashok Kumar and P. Dananjayan. “Improvement of Code Utilization CDMA for On-Chip Communication Architecture using Orthogonal Gold Code”. In: *Proceedings of the 3rd International Conference on Inventive Computation Technologies, ICICT 2018*. Institute of Electrical and Electronics Engineers Inc., 2018, pp. 567–571. ISBN: 9781538649855.
- [23] Petar Popovski, Hiroyuki Yomo, and Ramjee Prasad. “Strategies for adaptive frequency hopping in the unlicensed bands”. In: *IEEE Wireless Communications* 13.6 (2006), pp. 60–67. ISSN: 15361284.
- [24] Theodore Rappaport. *Wireless Communications: Principles and Practice*. Ed. by IEEE. 1996, p. 641.
- [25] Hermann Rohling and Matthias Kronauge. “New radar waveform based on a chirp sequence”. In: *2014 International Radar Conference, Radar 2014*. Institute of Electrical and Electronics Engineers Inc., 2014. ISBN: 9781479941957.
- [26] Qian Yang, Ran Tao, and Yue Wang. “Performance of chirp-based multicarrier system in narrowband interference”. In: *Proceedings - 2011 International Conference on Instrumentation, Measurement, Computer, Communication and Control, IMCCC 2011*. 2011, pp. 752–754. ISBN: 9780769545196.
- [27] Felix Wunsch, Holger Jäkel, and Friedrich K. Jondral. “Performance evaluation of IEEE 802.15.4 OQPSK and CSS PHY in the presence of interference”. In: *2015 IEEE 82nd Vehicular Technology Conference, VTC Fall 2015 - Proceedings*. Institute of Electrical and Electronics Engineers Inc., 2016. ISBN: 9781479980918.

-
- [28] Man Standards Committee of the IEEE Computer Society. *IEEE Std 802.15.4TM-2015, IEEE Standard for Low-Rate Wireless Networks*. 2016. ISBN: 9781504408462. URL: <http://www.ieee.org/web/aboutus/whatis/policies/p9-26.html>..
- [29] Lorenzo Vangelista. “Frequency Shift Chirp Modulation: The LoRa Modulation”. In: *IEEE Signal Processing Letters* 24.12 (2017), pp. 1818–1821. ISSN: 10709908.
- [30] Pavel I. Puzyrev, Maxim A. Kvachev, and Victor V. Erokhin. “Frequency Shift Chirp Modulation with Additional Differential Phase Shift Keying”. In: *International Conference of Young Specialists on Micro/Nanotechnologies and Electron Devices, EDM*. Vol. 2019-June. IEEE Computer Society, 2019, pp. 78–82. ISBN: 9781728117539.
- [31] Brecht Reynders and Sofie Pollin. “Chirp spread spectrum as a modulation technique for long range communication”. In: *2016 IEEE Symposium on Communications and Vehicular Technology in the Benelux, SCVT 2016*. Institute of Electrical and Electronics Engineers Inc., 2016. ISBN: 9781509043613.
- [32] T. T. Nguyen et al. “Efficient Design of Chirp Spread Spectrum Modulation for Low-Power Wide-Area Networks”. In: *IEEE Internet of Things Journal* 6.6 (2019), pp. 9503–9515.
- [33] Leon Kocjancic, Alessio Balleri, and Thomas Merlet. “Study of the frequency slope effect on the chirp waveform orthogonality”. In: *IET Conference Publications*. Vol. 2017. CP728. Institution of Engineering and Technology, 2017. ISBN: 9781785614217.
- [34] *US8406275B2 - Communications system - Google Patents*. URL: <https://patents.google.com/patent/US8406275B2/en> (visited on 07/17/2020).
- [35] Semtech Corporation. “No Title”. Camarillo, CA, USA, 2013.
- [36] LoRa Alliance Technical Committee. “LoRaWAN® Specification v1.1 | LoRa Alliance®”. URL: <https://lora-alliance.org/resource-hub/lorawanr-specification-v11>.
- [37] Man Standards Committee of the IEEE Computer Society. *IEEE Std 802.15.4TM-2015, IEEE Standard for Low-Rate Wireless Networks*. 2016. ISBN: 9781504408462.
- [38] *File:LoRa end-devices activation.png - Wikimedia Commons*. URL: <https://commons.wikimedia.org/w/index.php?curid=82331716> (visited on 09/23/2020).

-
- [39] Abdelfatteh Lachtar, Thierry Val, and Abdennaceur Kachouri. “Elderly monitoring system in a smart city environment using LoRa and MQTT”. In: *IET Wireless Sensor Systems* 10.2 (2020), pp. 70–77. ISSN: 20436394.
- [40] *Ageing / United Nations*. URL: <https://www.un.org/en/sections/issues-depth/ageing/> (visited on 07/24/2020).
- [41] United Nations Department of Economic, Social Affairs, and Population Division. *World Population Ageing 2019*. Tech. rep. 2019.
- [42] *Alzheimer’s Facts and Figures Report / Alzheimer’s Association*. URL: <https://www.alz.org/alzheimers-dementia/facts-figures> (visited on 07/24/2020).
- [43] Ming-Chyi Pai and Chih-Chien Lee. “The Incidence and Recurrence of Getting Lost in Community-Dwelling People with Alzheimer’s Disease: A Two and a Half-Year Follow-Up”. In: *PLOS ONE* 11.5 (2016). Ed. by Alexander N. Sokolov, e0155480. ISSN: 1932-6203. URL: <https://dx.plos.org/10.1371/journal.pone.0155480>.
- [44] Vincenzo Della Mea et al. “A Communication Infrastructure for the Health and Social Care Internet of Things: Proof-of-Concept Study”. In: *JMIR Medical Informatics* 8.2 (2020), e14583. ISSN: 2291-9694. URL: <https://pubmed.ncbi.nlm.nih.gov/32130158/>.
- [45] Afef Mdhaffar et al. “IoT-based health monitoring via LoRaWAN”. In: *17th IEEE International Conference on Smart Technologies, EUROCON 2017 - Conference Proceedings*. Institute of Electrical and Electronics Engineers Inc., 2017, pp. 519–524. ISBN: 9781509038435.
- [46] Juha Petajarvi et al. “Evaluation of LoRa LPWAN technology for remote health and wellbeing monitoring”. In: *International Symposium on Medical Information and Communication Technology, ISMICT*. Vol. 2016-June. IEEE Computer Society, 2016. ISBN: 9781509028498.
- [47] Alagumeenaakshi Muthiah et al. “Maternal ehealth Monitoring System using LoRa Technology”. In: *2019 IEEE 10th International Conference on Awareness Science and Technology, iCAST 2019 - Proceedings*. Institute of Electrical and Electronics Engineers Inc., 2019. ISBN: 9781728138213.
- [48] *Semtech’s LoRa® Devices Integrated into Polysense’s Infrared Temperature Sensor*. URL: <https://www.semtech.com/company/press/semtechs-lora-devices-integrated-into-polysenses-infrared-temperature-sensor> (visited on 07/24/2020).

-
- [49] *Semtech and LoRaWAN Ecosystem Members Deliver LoRa®-based Solutions to Optimize Health Services in China*. URL: <https://www.semtech.com/company/press/semtech-and-lorawan-ecosystem-members-deliver-lora-based-solutions-to-optimize-health-services-in-china> (visited on 07/24/2020).
- [50] *CareBand Launches COVID-19 People Safety Solutions*. Tech. rep.
- [51] *Air pollution*. URL: https://www.who.int/health-topics/air-pollution{\#}tab=tab{_}1 (visited on 07/25/2020).
- [52] *Ambient (outdoor) air pollution*. URL: [https://www.who.int/news-room/fact-sheets/detail/ambient-\(outdoor\)-air-quality-and-health](https://www.who.int/news-room/fact-sheets/detail/ambient-(outdoor)-air-quality-and-health) (visited on 07/25/2020).
- [53] L. Angrisani et al. “An innovative air quality monitoring system based on drone and iot enabling technologies”. In: *2019 IEEE International Workshop on Metrology for Agriculture and Forestry, MetroAgriFor 2019 - Proceedings*. Institute of Electrical and Electronics Engineers Inc., 2019, pp. 207–211. ISBN: 9781728136110.
- [54] Siwen Liu, Xufei Yang, and Xiaobing Zhou. “Development of a low-cost UAV-based system for CH₄ monitoring over oil fields”. In: *Environmental Technology* (2020), pp. 1–10. ISSN: 0959-3330. URL: <https://www.tandfonline.com/doi/full/10.1080/09593330.2020.1724199>.
- [55] Koichiro Ishibashi et al. “Beat sensors for smart environment monitoring systems”. In: *Proceedings - 2019 3rd International Conference on Recent Advances in Signal Processing, Telecommunications and Computing, SigTelCom 2019*. Institute of Electrical and Electronics Engineers Inc., 2019, pp. 77–79. ISBN: 9781538679630.
- [56] Steven J. Johnston et al. “City Scale Particulate Matter Monitoring Using LoRaWAN Based Air Quality IoT Devices”. In: *Sensors* 19.1 (2019), p. 209. ISSN: 1424-8220. URL: <https://www.mdpi.com/1424-8220/19/1/209>.
- [57] Yushuang Ma et al. “Development and Application of an Atmospheric Pollutant Monitoring System Based on LoRa—Part I: Design and Reliability Tests”. In: *Sensors* 18.11 (2018), p. 3891. ISSN: 1424-8220. URL: <http://www.mdpi.com/1424-8220/18/11/3891>.
- [58] Vishal Choudhary et al. “AirQ: A Smart IoT Platform for Air Quality Monitoring”. In: *2020 IEEE 17th Annual Consumer Communications and Networking Conference, CCNC 2020*. Institute of Electrical and Electronics Engineers Inc., 2020. ISBN: 9781728138930.

- [59] Rizky Firdaus, Muhammad Ary Murti, and Ibnu Alinursafa. “Air quality monitoring system based internet of things (IoT) using LPWAN LoRa”. In: *Proceedings - 2019 IEEE International Conference on Internet of Things and Intelligence System, IoTaIS 2019*. Institute of Electrical and Electronics Engineers Inc., 2019, pp. 195–200. ISBN: 9781728125169.
- [60] Varada Raju, Addala Satya Narayana Varma, and Y. Satyanarayana Raju. “An environmental pollution monitoring system using LORA”. In: *2017 International Conference on Energy, Communication, Data Analytics and Soft Computing, ICECDS 2017*. Institute of Electrical and Electronics Engineers Inc., 2018, pp. 3521–3526. ISBN: 9781538618868.
- [61] Rahayu Dwi Lestari et al. “Design of IoT-based river water monitoring robot data transmission model using low power wide area network (LPWAN) communication technology”. In: *Proceedings - 2019 IEEE International Conference on Internet of Things and Intelligence System, IoTaIS 2019*. Institute of Electrical and Electronics Engineers Inc., 2019, pp. 201–205. ISBN: 9781728125169.
- [62] Md Eshrat E. Alahi et al. “An Internet-of-Things Enabled Smart Sensing System for Nitrate Monitoring”. In: *IEEE Internet of Things Journal* 5.6 (2018), pp. 4409–4417. ISSN: 23274662.
- [63] Ernesto Leon et al. “Flood Early Warning System by Twitter Using LoRa”. In: *Proceedings* 2.19 (2018), p. 1213. ISSN: 2504-3900. URL: <http://www.mdpi.com/2504-3900/2/19/1213>.
- [64] Errynando Surya Sasmita, Mia Rosmiati, and Moch Fahru Rizal. “Integrating Forest Fire Detection with Wireless Sensor Network Based on Long Range Radio”. In: *Proceedings - 2018 International Conference on Control, Electronics, Renewable Energy and Communications, ICCEREC 2018*. Institute of Electrical and Electronics Engineers Inc., 2018, pp. 222–225. ISBN: 9781728119939.
- [65] Adnan et al. “Forest Fire Detection using LoRa Wireless Mesh Topology”. In: *Proceedings - 2nd East Indonesia Conference on Computer and Information Technology: Internet of Things for Industry, EIconCIT 2018*. Institute of Electrical and Electronics Engineers Inc., 2018, pp. 184–187. ISBN: 9781538680483.
- [66] Roberto Vega-Rodriguez et al. “Low Cost LoRa based Network for Forest Fire Detection”. In: *2019 6th International Conference on Internet of Things: Systems, Management and Security, IOTSMS 2019*. Institute of Electrical and Electronics Engineers Inc., 2019, pp. 177–184. ISBN: 9781728129495.

-
- [67] Rihab Fekih Romdhane et al. “Wireless sensors network for landslides prevention”. In: *2017 IEEE International Conference on Computational Intelligence and Virtual Environments for Measurement Systems and Applications, CIVEMSA 2017 - Proceedings*. Institute of Electrical and Electronics Engineers Inc., 2017, pp. 222–227. ISBN: 9781509042524.
- [68] Shadia Awadallah, David Moure, and Pedro Torres-González. “An Internet of Things (IoT) Application on Volcano Monitoring”. In: *Sensors* 19.21 (2019), p. 4651. ISSN: 1424-8220. URL: <https://www.mdpi.com/1424-8220/19/21/4651>.
- [69] Daeun Yim et al. “An experimental LoRa performance evaluation in tree farm”. In: *2018 IEEE Sensors Applications Symposium, SAS 2018 - Proceedings*. Vol. 2018-Janua. Institute of Electrical and Electronics Engineers Inc., 2018, pp. 1–6. ISBN: 9781538620922.
- [70] Marcus Hardie and Donald Hoyle. “Underground Wireless Data Transmission Using 433-MHz LoRa for Agriculture”. In: *Sensors* 19.19 (2019), p. 4232. ISSN: 1424-8220. URL: <https://www.mdpi.com/1424-8220/19/19/4232>.
- [71] Maksudjon Usmonov and Francesco Gregoretti. “Design and implementation of a LoRa based wireless control for drip irrigation systems”. In: *2017 2nd International Conference on Robotics and Automation Engineering, ICRAE 2017*. Vol. 2017-Decem. Institute of Electrical and Electronics Engineers Inc., 2018, pp. 248–253. ISBN: 9781538613054.
- [72] Ravi Kishore Kodali, Subbachari Yerroju, and Shubhi Sahu. “Smart Farm Monitoring Using LoRa Enabled IoT”. In: *Proceedings of the 2nd International Conference on Green Computing and Internet of Things, ICGCIoT 2018*. Institute of Electrical and Electronics Engineers Inc., 2018, pp. 391–394. ISBN: 9781538656570.
- [73] Juha Petäjäjärvi et al. “Performance of a low-power wide-area network based on LoRa technology: Doppler robustness, scalability, and coverage”. In: *Research Article International Journal of Distributed Sensor Networks* 13.3 (2017), p. 2017. URL: <http://www.uk.sagepub.com/aboutus/>.
- [74] Andrew Mackey, Petros Spachos, and Stefano Gregori. “Energy Efficient Bike-Share Tracking System with BLE Beacons and LoRa Technology”. In: *2019 IEEE Sustainability through ICT Summit, StICT 2019*. Institute of Electrical and Electronics Engineers Inc., 2019. ISBN: 9781728103082.

- [75] C. Ambika Bhuvanewari and M. Muthumari. “Design and realization of radio communication using LoRa & XBee module for an e-Bike”. In: *2018 IEEE International Conference on Computational Intelligence and Computing Research, ICCIC 2018*. Institute of Electrical and Electronics Engineers Inc., 2018. ISBN: 9781538615072.
- [76] José Santa et al. “LPWAN-Based Vehicular Monitoring Platform with a Generic IP Network Interface”. In: *Sensors* 19.2 (2019), p. 264. ISSN: 1424-8220. URL: <http://www.mdpi.com/1424-8220/19/2/264>.
- [77] Sappasit Thongmee and Nithiroth Pornsuwancharoen. “The Intelligent Automobile Applied a Vehicular Ad-Hoc Network by the microcontroller”. In: *Proceedings of 2019 2nd World Symposium on Communication Engineering, WSCE 2019*. Institute of Electrical and Electronics Engineers Inc., 2019, pp. 220–224. ISBN: 9781728153292.
- [78] Flavio Chaffo, Percy Saravia, and Guillermo Kemper. “A Wireless Communication Device Based on Lora Module Aimed at Detecting Rectilinear Proximity between Vehicles”. In: *2019 Congreso Internacional de Innovacion y Tendencias en Ingenieria, CONIITI 2019 - Conference Proceedings*. Institute of Electrical and Electronics Engineers Inc., 2019. ISBN: 9781728147468.
- [79] S. Manivannan and E. Kaleeswaran. “Solar powered electric vehicle”. In: *2016 1st International Conference on Sustainable Green Buildings and Communities, SGBC 2016*. Institute of Electrical and Electronics Engineers Inc., 2017. ISBN: 9781509034987.
- [80] Anisa Dewi Prajanti et al. “Performance Analysis of LoRa WAN Technology for Optimum Deployment of Jakarta Smart City”. In: *2018 2nd International Conference on Informatics and Computational Sciences, ICICoS 2018*. Institute of Electrical and Electronics Engineers Inc., 2019, pp. 54–59. ISBN: 9781538674406.
- [81] Gianni Pasolini et al. “Smart City Pilot Projects Using LoRa and IEEE802.15.4 Technologies”. In: *Sensors* 18.4 (2018), p. 1118. ISSN: 1424-8220.
- [82] Silvano Bertoldo et al. “Feasibility Study of LoRa Ad-Hoc Network in an Urban Noisy Environment”. In: *Mediterranean Microwave Symposium*. Vol. 2018-Octob. IEEE Computer Society, 2019, pp. 357–360. ISBN: 9781538671320.

- [83] Huang Chen Lee and Kai Hsiang Ke. “Monitoring of Large-Area IoT Sensors Using a LoRa Wireless Mesh Network System: Design and Evaluation”. In: *IEEE Transactions on Instrumentation and Measurement* 67.9 (2018), pp. 2177–2187. ISSN: 00189456.
- [84] Sebastian Meiling and Thomas C. Schmidt. “LoRa in the Field: Insights from Networking the Smart City Hamburg with RIOT”. In: (2020). arXiv: 2003.08647. URL: <http://arxiv.org/abs/2003.08647>.
- [85] Mohammed Saleh Ali Muthanna et al. “Development of intelligent street lighting services model based on LoRa technology”. In: *Proceedings of the 2018 IEEE Conference of Russian Young Researchers in Electrical and Electronic Engineering, ElConRus 2018*. Vol. 2018-Janua. Institute of Electrical and Electronics Engineers Inc., 2018, pp. 90–93. ISBN: 9781538643396.
- [86] Matteo Cerchecci et al. “A Low Power IoT Sensor Node Architecture for Waste Management Within Smart Cities Context”. In: *Sensors* 18.4 (2018), p. 1282. ISSN: 1424-8220.
- [87] Fowzia Akhter et al. “IoT Enabled Intelligent Sensor Node for Smart City: Pedestrian Counting and Ambient Monitoring”. In: *Sensors* 19.15 (2019), p. 3374. ISSN: 1424-8220.
- [88] Petar Solic et al. “Proof of Presence: Novel Vehicle Detection System”. In: *IEEE Wireless Communications* 26.6 (2019), pp. 44–49. ISSN: 15580687.
- [89] *IBM News room - 2011-09-28 IBM Global Parking Survey: Drivers Share Worldwide Parking Woes - United States*. URL: <https://www-03.ibm.com/press/us/en/pressrelease/35515.wss> (visited on 09/16/2020).
- [90] Andrea Abrardo and Alessandro Pozzebon. “A Multi-Hop LoRa Linear Sensor Network for the Monitoring of Underground Environments: The Case of the Medieval Aqueducts in Siena, Italy”. In: *Sensors* 19.2 (2019), p. 402. ISSN: 1424-8220.
- [91] Michifumi Miyashita. “Evaluation of Wireless Communication for Maintenance of Underground Power Transmission Lines”. In: *7th International Conference on Smart Grid, icSmartGrid 2019*. Institute of Electrical and Electronics Engineers Inc., 2019, pp. 81–86. ISBN: 9781728148588.
- [92] Weitao Xu et al. “Measurement, Characterization, and Modeling of LoRa Technology in Multifloor Buildings”. In: *IEEE Internet of Things Journal* 7.1 (2020), pp. 298–310. ISSN: 23274662. arXiv: 1909.03900.

-
- [93] Bashima Islam et al. “LoRaIn: Making a Case for LoRa in Indoor Localization”. In: *2019 IEEE International Conference on Pervasive Computing and Communications Workshops, PerCom Workshops 2019*. Institute of Electrical and Electronics Engineers Inc., 2019, pp. 423–426. ISBN: 9781538691519.
- [94] Hilmiey Hanaffi et al. “Single-Channel LoRaWAN Gateway for Remote Indoor Monitoring System: An Experimental”. In: *2020 8th International Electrical Engineering Congress, iEECON 2020*. Institute of Electrical and Electronics Engineers Inc., 2020. ISBN: 9781728130767.
- [95] Tingwei Wu, Dexin Qu, and Gengxin Zhang. “Research on LoRa adaptability in the LEO satellites internet of things”. In: *2019 15th International Wireless Communications and Mobile Computing Conference, IWCMC 2019*. Institute of Electrical and Electronics Engineers Inc., 2019, pp. 131–135. ISBN: 9781538677476.
- [96] Alexander A. Doroshkin et al. “Experimental Study of LoRa Modulation Immunity to Doppler Effect in CubeSat Radio Communications”. In: *IEEE Access* 7 (2019), pp. 75721–75731. ISSN: 21693536.
- [97] Giulio Colavolpe et al. “Reception of LoRa Signals from LEO Satellites”. In: *IEEE Transactions on Aerospace and Electronic Systems* 55.6 (2019), pp. 3587–3602. ISSN: 15579603.
- [98] Zhang Xuan et al. “An attempt to utilize lora for intersatellite communications”. In: *10th International Conference on Communications, Circuits and Systems, ICCAS 2018*. Institute of Electrical and Electronics Engineers Inc., 2018, pp. 260–264. ISBN: 9781538693872.
- [99] *SX1272 | Long Range, Low Power RF Transceiver 860-1000MHz | Semtech*. URL: <https://www.semtech.com/products/wireless-rf/lora-transceivers/sx1272> (visited on 11/04/2020).
- [100] *SX1276 | 137MHz to 1020MHz Long Range Low Power Transceiver | Semtech*. URL: <https://www.semtech.com/products/wireless-rf/lora-transceivers/sx1276> (visited on 11/04/2020).
- [101] *SX1261 | Long Range Low Power LoRa® RF Transceiver +15dBm | Semtech*. URL: <https://www.semtech.com/products/wireless-rf/lora-transceivers/sx1261> (visited on 11/04/2020).
- [102] A.G. Longley and P.L. Rice. *Prediction of Tropospheric Radio Transmission Loss Over Irregular Terrain: A Computer Method-1968*. Ed. by Institute for Telecommunication Sciences. 1968.
- [103] Itu-r. *Propagation by diffraction P Series Radiowave propagation*. Tech. rep. URL: <http://www.itu.int/ITU-R/go/patents/en>.

- [104] Masaharu Hata. “Empirical Formula for Propagation Loss in Land Mobile Radio Services”. In: *IEEE Trans. Veh. Technol.* 29.3 (1980), pp. 317–325. ISSN: 19399359.
- [105] *MINISTERO DELLE COMUNICAZIONI, ELENCO DELLE INTERFACCE PER GLI APPARATI RADIOELETTRICI, dal n. 1 al n. 66*. URL: https://www.gazzettaufficiale.it/atto/serie_generale/caricaArticolo?art.progressivo=0&art.idArticolo=1&art.versione=1&art.codiceRedazionale=05A00705&art.dataPubblicazioneGazzetta=2005-02-12&art.idGruppo=0&art.idSottoArticolo1=10&art.idSottoArticolo=1&art.flagTipoArticolo=1 (visited on 11/28/2020).
- [106] Andreas Molisch. *Wireless Communications*. Wiley-IEEE Press, 2005. ISBN: 047084888X.
- [107] J. S. Seybold. *Introduction to RF Propagation*. Wiley-Interscience, 2005. ISBN: 0471655961.
- [108] *Salesforce*. URL: https://semtech.my.salesforce.com/sfc/p/{\#}E0000000JelG/a/2R0000001Rbr/6EfVZUorrpoKFfvaF{_}Fkpgp5kzjiNyiAbqcpqh9qSjE (visited on 11/28/2020).
- [109] Itu-r. *Propagation data and prediction methods for the planning of indoor radiocommunication systems and radio local area networks in the frequency range 300 MHz to 100 GHz P Series Radiowave propagation*. Tech. rep. URL: <http://www.itu.int/ITU-R/go/patents/en>.
- [110] Michael Mollel and Michael Kisangiri. “Comparison of Empirical Propagation Path Loss Models for Mobile Communication”. In: *Computer Engineering and Intelligent Systems* 5 (Jan. 2014).
- [111] Pascal Jörke et al. “Urban channel models for smart city IoT-networks based on empirical measurements of LoRa-lmks at 433 and 868 MHz”. In: *IEEE Int. Symp. Pers. Indoor Mob. Radio Commun. PIMRC*. Vol. 2017-Octob. Institute of Electrical and Electronics Engineers Inc., 2018, pp. 1–6. ISBN: 9781538635315.
- [112] R. El Chall, S. Lahoud, and M. El Helou. “LoRaWAN Network: Radio Propagation Models and Performance Evaluation in Various Environments in Lebanon”. In: *IEEE Internet of Things Journal* 6.2 (2019), pp. 2366–2378.